Primordial gravitational waves in nonstandard cosmologies

Nicolás Bernal[1,*] and Fazlollah Hajkarim[2,†]

[1]*Centro de Investigaciones, Universidad Antonio Nariño, Carrera 3 Este # 47A-15, Bogotá, Colombia*
[2]*Institut für Theoretische Physik, Goethe Universität, Max von Laue Straße 1, D-60438 Frankfurt, Germany*

(Received 17 July 2019; published 3 September 2019)

Assuming that inflation is followed by a phase where the energy density of the Universe is dominated by a component with a general equation of state, we evaluate the spectrum of primordial gravitational waves induced in the postinflationary Universe. We show that if the energy density of the Universe is dominated by a component ϕ before big bang nucleosynthesis, its equation of state could be constrained by gravitational wave experiments depending on the ratio of energy densities of ϕ and radiation and also the temperature at the end of the ϕ-dominated era. Also, we discuss the impact of scale dependence of tensor modes on the primordial gravitational wave spectrum during the ϕ domination. These models are motivated by beyond Standard Model physics and scenarios for nonthermal production of dark matter in the early Universe. We also constrain the parameter space of the tensor spectral index and the tensor-to-scalar ratio, using the experimental limits from gravitational wave experiments.

DOI: 10.1103/PhysRevD.100.063502

I. INTRODUCTION

The recent observations of gravitational waves (GWs) by LIGO and Virgo [1–6] paved the way to observe the Universe with new methods not based on electromagnetic radiation. Until now our knowledge about the early Universe cosmology was limited by electromagnetic waves back to last scattering surface of photons, some possible effects of inflationary scenario on the cosmic microwave background (CMB), and the abundance of light elements from big bang nucleosynthesis (BBN). Although the current GW detectors are only sensitive to strong astrophysical events such as merging black holes or neutron stars, future experiments are expected to detect much weaker signatures produced in the early Universe [7,8]. Several space-borne interferometers such as the proposed ground-based Einstein Telescope (ET) [9], the planned space-based LISA [10] interferometer, the proposed successor experiments BBO [11], (B-)DECIGO [12,13], as well as the Square Kilometre Array (SKA) [14] telescope are planned to be operational in the future with the aim of detecting the primordial GW (PGW) background and the effect of possible cosmic phase transitions on it.

The existence of a PGW background is one of the most crucial predictions of the inflationary scenario of the early Universe [15,16]. The spectrum of the inflationary GWs that could be observed today depends on two main factors: one is the power spectrum of primordial tensor perturbations generated during inflation, and the other is the expansion rate of the Universe from the end of inflation until today. The former defines the initial magnitude of the GW signature, and it is directly associated with the detailed properties of inflationary models. The latter describes how the density of the PGWs has been diluted in subsequent stages of the cosmic expansion. Since the amplitude and polarization of PGWs can be modified by nonstandard cosmological scenarios, there is a possibility to extract information about the early Universe using GW experiments [17].

On the one hand, concerning the PGW spectrum, current CMB measurements do not have the ability to constrain the amplitude A_T nor the tensor spectral index n_T. The measurement of the tensor-to-scalar ratio r is still compatible with zero, and for low enough r, practically any value of n_T is still acceptable. For this reason, the constraints on n_T depend on the chosen prior on r. This situation will change when a positive detection of a nonzero tensor amplitude is obtained from primordial B modes [18,19].

On the other hand, several effects, like the decoupling of neutrinos or the variation of Standard Model (SM) relativistic degrees of freedom, alter the nature of the GW spectrum during its propagation [20–34]. However, one can imagine that instead of being dominated by radiation over its early phase (i.e. the standard cosmological scenario), the evolution of the Universe could have been driven by matter, or in general by a component ϕ with a general equation of state ω_ϕ. In fact, there are no fundamental reasons to

*nicolas.bernal@uan.edu.co
†hajkarim@th.physik.uni-frankfurt.de

assume that the Universe was radiation dominated prior to BBN[1] at $t \sim 1$ s. Studying what consequences such a nonstandard era can have on observational properties of GWs is hence worthwhile. In particular, GWs in scenarios with an early matter era have received particular attention [42–47]. Additionally, let us note that production of dark matter in scenarios with nonstandard expansion phases has recently gained increasing interest [48–83].

Previous works have already investigated the degree to which the thermal history and the early Universe equation of state affect the propagation of GWs [23,27,28,34,84–95] and also how the pre-BBN Universe could be probed with GWs from cosmic strings [96,97] or from gravitational reheating [98]. Instead, here we perform a full numerical evaluation of the PGW spectrum, solving properly the equations for the background energy density and taking special care of the variation of the SM degrees of freedom. For different PGW spectra and varying the possible thermal histories of the Universe, we explore the capabilities of current and future GW detectors to probe the GW background.

The rest of this paper is organized as follows. In Sec. II we revisit the set of differential equations that govern the tensor perturbations. Then we compute the spectrum of GWs in the standard radiation-dominated period. In Sec. III we introduce our setup for nonstandard cosmologies to include possible equations of state for the fluid ϕ and their impact on the Hubble expansion rate and the thermal history of the Universe. Section IV is devoted to the calculation of a relic GW spectrum in the case of a scale-invariant power spectrum and assuming a ϕ-dominated era. We also perform a scan over the parameter space of possible equations of state and ratio of densities for radiation and the nonstandard fluid. The effect of scale dependence on the spectrum of GWs on the parameter space is also studied. Finally, we conclude and summarize our results in Sec. V.

II. PRIMORDIAL GRAVITATIONAL WAVE SPECTRUM

GWs are represented by spatial metric perturbations that satisfy the transverse-traceless conditions: $\partial^i h_{ij} = 0$ and $h^i_i = 0$. The evolution of GWs is described by the linearized Einstein equation

$$\ddot{h}_{ij} + 3H\dot{h}_{ij} - \frac{\nabla^2}{a^2} h_{ij} = 16\pi G \Pi^{TT}_{ij}, \tag{2.1}$$

where the dots correspond to derivatives with respect to the cosmic time t and G is the Newton's constant. Π^{TT}_{ij} is the transverse-traceless part of the anisotropic stress tensor Π_{ij},

$$\Pi_{ij} = \frac{T_{ij} - p g_{ij}}{a^2}, \tag{2.2}$$

where T_{ij} is the stress-energy tensor, g_{ij} is the metric tensor and p is the background pressure. The spatial metric perturbations can be decomposed into their Fourier modes

$$h_{ij}(t, \vec{x}) = \sum_\lambda \int \frac{d^3k}{(2\pi)^3} h^\lambda(t, \vec{k}) \epsilon^\lambda_{ij}(\vec{k}) e^{i\vec{k}\cdot\vec{x}}, \tag{2.3}$$

where $\lambda = +, \times$ corresponds to the two independent polarization states and $\epsilon^\lambda_{ij}(\vec{k})$ are the spin-2 polarization tensors satisfying the normalization conditions $\sum_{ij} \epsilon^\lambda_{ij} \epsilon^{\lambda' *}_{ij} = 2\delta^{\lambda\lambda'}$. Equation (2.1) can therefore be rewritten as

$$\ddot{h}^\lambda_{\vec{k}} + 3H\dot{h}^\lambda_{\vec{k}} + \frac{k^2}{a^2} h^\lambda_{\vec{k}} = 16\pi G \Pi^\lambda_{\vec{k}}, \tag{2.4}$$

where $h^\lambda_{\vec{k}}(t) \equiv h^\lambda(t, \vec{k})$. In the rest of this paper we consider the rhs of the above equation to be zero so it does not enhance the primordial tensor perturbations. However, in general it is finite, for example when one considers the effect of damping of photons and neutrinos at low frequencies or the impact of scalar perturbations which can act as a source for tensor perturbations [8,90,99]. We do not consider such effects in this paper. The solution of Eq. (2.4) can be expressed as

$$h^\lambda_{\vec{k}} = h^\lambda_{\vec{k},\mathrm{prim}} X(t, k), \tag{2.5}$$

where $h^\lambda_{\vec{k},\mathrm{prim}}$ represents the amplitude of the primordial tensor perturbations and $X(t, k)$ is the transfer function, normalized such that $X(t, k) = 1$ for $k \ll aH$.

The energy density of the relic GWs is given by

$$\rho_{\mathrm{GW}}(t) = \frac{1}{16\pi G} \sum_\lambda \int \frac{d^3k}{(2\pi)^3} |\dot{h}^\lambda_{\vec{k}}|^2. \tag{2.6}$$

The primordial gravitational wave spectrum is calculated following Refs. [28,90]:

$$\Omega_{\mathrm{GW}}(t, k) = \frac{1}{\rho_c(t)} \frac{d\rho_{\mathrm{GW}}(t, k)}{d \ln k}, \tag{2.7}$$

where ρ_c is the critical energy density of the Universe. This spectrum can be rewritten using Eq. (2.5) as

$$\Omega_{\mathrm{GW}}(\eta, k) = \frac{1}{12 a^2(\eta) H^2(\eta)} \mathcal{P}_T(k) [X'(\eta, k)]^2, \tag{2.8}$$

where the prime represents the derivative with respect to the conformal time η. The primordial tensor power spectrum $\mathcal{P}_T(k)$ is determined by the Hubble parameter at the time

[1]For studies on baryogenesis with a low reheating temperature or during an early matter-dominated phase, see Refs. [35–40] and [41], respectively.

when the corresponding mode crosses the horizon during inflation, at $k = aH$:

$$\mathcal{P}_T(k) \equiv \frac{k^3}{\pi^2}\sum_{\lambda}|h^{\lambda}_{\vec{k},\mathrm{prim}}|^2 = \left.\frac{2H^2}{\pi^2 M_{\mathrm{Pl}}^2}\right|_{k=aH}, \tag{2.9}$$

where $M_{\mathrm{Pl}} = 2.435 \times 10^{18}$ GeV is the reduced Planck mass.

The transfer function is found by numerically solving the equation

$$\frac{d^2X(u)}{du^2} + \frac{2}{a(u)}\frac{da(u)}{du}\frac{dX(u)}{du} + X(u) = 0, \tag{2.10}$$

where $u \equiv k\eta$. Again, although the shear of the cosmic fluid gives rise to some important effects [28], we ignore its possible contribution by setting the rhs of Eq. (2.10) to zero, for frequencies beyond $\sim 10^{-10}$ Hz. In the frequency range between $\sim 10^{-16}$ and $\sim 10^{-10}$ Hz, the damping effect due to the free-streaming neutrinos reduce the amplitude of GWs by ∼35% [20,21,24], which is not interesting for us in this paper. The initial conditions are specified as

$$X(0) = 1, \qquad \frac{dX}{du}(0) = 0. \tag{2.11}$$

The wave equation (2.10) is solved up to some finite time u' after horizon crossing; after that we extrapolate the solution until the present time by using the WKB solution:

$$X(u) = \frac{A}{a(u)}\sin(u + \delta), \tag{2.12}$$

where A and δ are fixed such that X and dX/du match the numerical solution at $u = u'$.

Figure 1 shows the result of the numerical integration of the spectrum of inflationary GWs as a function of the frequency $f \equiv k/(2\pi)$, for the standard cosmological scenario. We have fixed the inflationary scale as $V_{\mathrm{inf}}^{1/4} = 1.5 \times 10^{16}$ GeV,[2] i.e. $\mathcal{P}_T(k) = \frac{2}{3\pi^2}\frac{V_{\mathrm{inf}}}{M_{\mathrm{Pl}}^4}$, and assume a primordial scale-invariant scenario, i.e. $n_T = 0$ (also see Sec. IV A 6). We also show the temperature T_{hc} at which the corresponding mode reenters the horizon. The oscillatory behavior is a genuine feature of inflationary GWs. The decrease in the spectrum between $\sim 10^{-9}$ and $\sim 10^{-8}$ Hz corresponds to the variation of the relativistic degrees of freedom due to the QCD smooth crossover transition, where we used the SM equation of state from Ref. [101]. Moreover, it was shown that using a different lattice QCD equation of state for the calculation of the SM equation of state only affects the predicted PGW spectrum

[2]This value comes from the fact that at the end of inflation after 60 e-folds the value of Hubble parameter is $H_{\mathrm{inf}} \sim 10^{-5} M_{\mathrm{Pl}}$ [100].

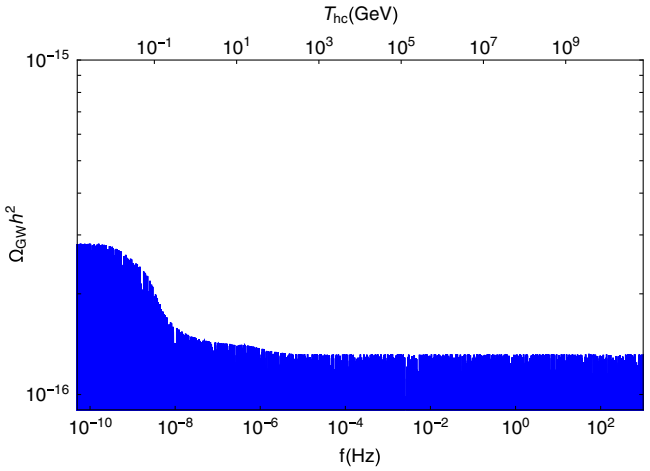

FIG. 1. The spectrum of inflationary GWs ($\Omega_{\mathrm{GW}}h^2$) as a function of the frequency f, for the standard cosmological scenario. Here we fix the inflationary scale as $V_{\mathrm{inf}}^{1/4} = 1.5 \times 10^{16}$ GeV and assume a primordial scale-invariant spectrum, i.e. $n_T = 0$. We also show the temperature T_{hc} at which the corresponding mode reenters the horizon.

at the order of a few percent [102,103]. The dependence on the number of relativistic degrees of freedom $g_\star$ and $h_\star$ that contribute to the SM energy density and the SM entropy density, respectively, is [90]

$$\Omega_{\mathrm{GW}}(\eta_0, k) \approx \frac{\Omega_\gamma(T_0)}{48} g_\star(T_{\mathrm{hc}}) \left[\frac{h_\star(T_0)}{h_\star(T_{\mathrm{hc}})}\right]^{4/3} \mathcal{P}_T(k). \tag{2.13}$$

Here Ω_γ corresponds to the photon relic density, and T_0 and T_{hc} correspond to today's and horizon crossing temperatures, respectively.

III. NONSTANDARD COSMOLOGIES

We assume that for some period of the early Universe, the total energy density was dominated by a component ρ_ϕ with an equation of state parameter ω_ϕ, where $\omega_\phi \equiv p_\phi/\rho_\phi$, with p_ϕ the pressure of the dominant component. We assume that this component decays solely into SM radiation with a rate Γ_ϕ. In the early Universe, the evolution of the energy density ρ_ϕ and the SM entropy density s_R are governed by the system of coupled Boltzmann equations

$$\frac{d\rho_\phi}{dt} + 3(1 + \omega_\phi)H\rho_\phi = -\Gamma_\phi\rho_\phi, \tag{3.1}$$

$$\frac{ds_R}{dt} + 3Hs_R = +\frac{\Gamma_\phi\rho_\phi}{T}. \tag{3.2}$$

Under the assumption that the SM plasma maintains internal equilibrium at all times in the early Universe, the temperature dependence of the SM energy density ρ_R can be obtained from

$$\rho_R(T) = \frac{\pi^2}{30} g_\star(T) T^4. \tag{3.3}$$

Equation (3.2) plays an important role in tracking properly the evolution of the photon's temperature T, via the SM entropy density s_R:

$$s_R(T) = \frac{\rho_R + p_R}{T} = \frac{2\pi^2}{45} h_\star(T) T^3, \tag{3.4}$$

where $g_\star(T)$ and $h_\star(T)$ correspond to the effective number of relativistic degrees of freedom for the SM energy and entropy densities, respectively [101]. The Hubble expansion rate H is defined by

$$H^2 = \frac{\rho_\phi + \rho_R + \rho_m + \rho_\Lambda}{3M_{\rm Pl}^2}, \tag{3.5}$$

where ρ_m and ρ_Λ, corresponding to the matter and cosmological constant energy densities, respectively, are subdominant before the matter-radiation equality.

Using entropy conservation in standard cosmology we can compute the evolution of the temperature with respect to the scale factor using

$$\frac{dT}{da} = \left[1 + \frac{T}{3h_\star}\frac{dh_\star}{dT}\right]^{-1}\left[-\frac{T}{a}\right]. \tag{3.6}$$

However, once we assume a period of ϕ domination which decays to radiation the entropy is not conserved anymore and from Eqs. (3.2) and (3.4) one has

$$\frac{dT}{da} = \left[1 + \frac{T}{3h_\star}\frac{dh_\star}{dT}\right]^{-1}\left[-\frac{T}{a} + \frac{\Gamma_\phi \rho_\phi}{3Hsa}\right]. \tag{3.7}$$

The approximate temperature $T_{\rm dec}$ at which ϕ decays is fixed by the total decay width Γ_ϕ as

$$T_{\rm dec}^4 = \frac{90}{\pi^2 g_\star(T_{\rm dec})} M_{\rm Pl}^2 \Gamma_\phi^2. \tag{3.8}$$

For having a successful BBN, that temperature has to be $T_{\rm dec} \gtrsim T_{\rm BBN} \sim 4$ MeV [104–108]. To present the maximal effect that a nonstandard expansion phase can have on the GW spectrum, we choose $T_{\rm dec} = 10$ MeV, which is close to the BBN bound.[3] However, the results can be easily generalized to higher values of $T_{\rm dec}$. The scale factor at the moment when ϕ decays is denoted by $a_{\rm dec}$.

The initial condition used to compute the evolution of Boltzmann equations is

$$\xi \equiv \left.\frac{\rho_\phi}{\rho_R}\right|_{T=T_{\rm max}} \tag{3.9}$$

with $T_{\rm max} = 10^{14}$ GeV. In complete inflationary scenarios ξ is a theoretical prediction and not an input parameter. Let us emphasize that the choice of $T_{\rm max}$ is not physical, and therefore it should be taken as a simple pivot scale from which we start to solve the Boltzmann equations, and not as the maximal temperature reached by the thermal bath. The total energy density at $T = T_{\rm max}$ is the sum of radiation and ϕ, so that $\rho(T_{\rm max}) = (\rho_R + \rho_\phi)|_{T=T_{\rm max}} = \rho_R(T_{\rm max}) \times (1+\xi)$. We solve Eqs. (3.1) and (3.7) numerically to find the evolution of temperature with respect to scale factor in a nonstandard cosmological scenario. The scale factor a as a function of conformal time η can then be used as input for Eq. (2.10) to calculate the spectrum of the GW background under a ϕ-dominated era.

As an example, Fig. 2 shows the evolution of the energy densities ρ_R and ρ_ϕ as a function of the scale factor a, for $\omega_\phi = 0$ and $\xi = 10^{-11}$ (upper panel), $\omega_\phi = 1/3$ and $\xi = 10^{25}$ (central panel), and $\omega_\phi = 2/3$ and $\xi = 10^{10}$ (lower panel). We have chosen $T_{\rm dec} = 10$ MeV. In Fig. 2 the value of radiation energy density at $T = T_0$ (i.e. $a = a_0 = 1$) matches the CMB energy density. If one ignores the variation of the number of relativistic degrees of freedom $g_\star$ and $h_\star$, one has that $\rho_\phi(a) \propto a^{-3(1+\omega_\phi)}$ until it decays, and

$$\rho_R(a) \propto \begin{cases} a^{-4} & \text{for } a \ll a_{\rm start}, \\ a^{-\frac{3}{2}(1+\omega_\phi)} & \text{for } a_{\rm start} \ll a \ll a_{\rm dec}, \\ a^{-4} & \text{for } a_{\rm dec} \ll a, \end{cases} \tag{3.10}$$

which by using Eq. (3.3) implies that

$$T(a) \propto \begin{cases} a^{-1} & \text{for } a \ll a_{\rm start}, \\ a^{-\frac{3}{8}(1+\omega_\phi)} & \text{for } a_{\rm start} \ll a \ll a_{\rm dec}, \\ a^{-1} & \text{for } a_{\rm dec} \ll a. \end{cases} \tag{3.11}$$

Additionally, let us define $T_{\rm eq} \equiv T(a = a_{\rm eq})$, $T_{\rm start} \equiv T(a = a_{\rm start})$ and $T_{\rm end} \equiv T(a = a_{\rm end})$ (see the Appendix). $T_{\rm dec}$ is properly defined in Eq. (3.8). $T_{\rm eq}$ corresponds to the temperature at which $\rho_\phi = \rho_R$, well before ϕ decays, in the case where $\omega_\phi < 1/3$. In Fig. 2 the vertical gray lines corresponding to $a = a_{\rm eq}$, $a_{\rm start}$ and $a_{\rm end}$ are overlaid. Moreover, in Fig. 2 and in the rest of the paper we choose the normalization for which $a_0 \equiv a(T_0) = 1$.

This nonstandard scenario tends to converge to the usual radiation-dominated case when ξ takes small values. In fact, if $\xi \ll \xi_{\rm min}$, where

$$\xi_{\rm min} \approx \left[\left(\frac{g_\star(T_{\rm max})}{g_\star(T_{\rm dec})}\right)^{\frac{1}{4}} \frac{T_{\rm max}}{T_{\rm dec}}\right]^{3\omega_\phi - 1}, \tag{3.12}$$

[3]Let us note that for $\omega_\phi > 1/3$, ρ_ϕ gets dissolved faster than radiation. If $\rho_\phi \ll \rho_R$ at $T_{\rm dec}$, Γ_ϕ could effectively be taken to zero.

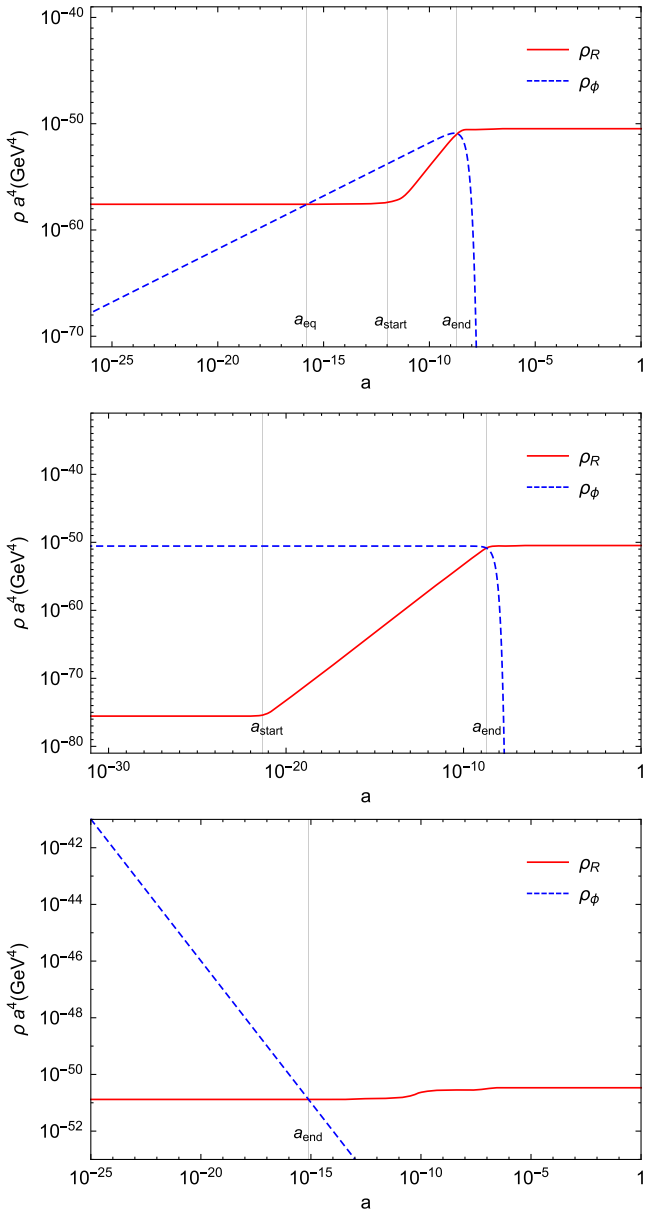

FIG. 2. Example of the evolution of the energy densities ρ_R and ρ_ϕ as a function of the scale factor a, for $\omega_\phi = 0$ and $\xi = 10^{-11}$ (upper panel), $\omega_\phi = 1/3$ and $\xi = 10^{25}$ (central panel), and $\omega_\phi = 2/3$ and $\xi = 10^{10}$ (lower panel). We have chosen $T_{\rm dec} = 10$ MeV. These benchmark points are the same used in Fig. 3 and are shown in the upper left panel of Fig. 4. The vertical gray lines corresponding to $a = a_{\rm eq}$, $a_{\rm start}$ and $a_{\rm end}$ are overlaid.

the period when the SM energy density scales like $a^{-\frac{3}{2}(1+\omega_\phi)}$ tends to disappear.[4] If $\omega_\phi < 1/3$, this corresponds to the case where ρ_R is always subdominant with respect to ρ_ϕ. In the opposite case, when $\omega_\phi > 1/3$, ϕ decays when its energy density is already subdominant.

[4]In the Appendix the criterion for defining $\xi_{\rm min}$ is presented.

IV. PRIMORDIAL GRAVITATIONAL WAVES IN NONSTANDARD COSMOLOGIES

In this paper we consider scenarios where for some period at early times the expansion of the Universe was governed by a fluid component with an effective equation of state ω_ϕ. Particular cases correspond to $\omega_\phi = -1$ (quintessence), 0 (matter, modulus), $1/3$ (radiation), and 1 (kination); however we consider general cases where $\omega_\phi \in [0, 1]$ in our numerical analysis. During the epoch when ϕ dominates the energy density of the Universe, the scale factor goes like $a(u) \propto u^{\frac{2}{3\omega_\phi+1}}$, in contrast to the standard case (i.e. radiation dominated), where $a(u) \propto u$. Therefore, the friction term in Eq. (2.10) leads to more or less damping than in the usual radiation case. It can be estimated to be

$$\frac{2}{a(u)}\frac{da}{du} \sim \frac{4}{3\omega_\phi + 1}\frac{1}{u}, \tag{4.1}$$

so that for $\omega_\phi > 1/3$ the friction term is reduced with respect to the usual scenario. In these cases, the spectrum of GWs can be enhanced. In the next sections we also consider the effect of tensor tilt n_T on the power spectrum which can boost or damp the power spectrum at high frequencies.

We should emphasize that these nonstandard cosmological scenarios are viable from the perspective of CMB data. This can be identified by using the range of variation of the number of e-folds N on the scalar spectral index n_s and the tensor-to-scalar ratio r. For slow-roll inflation, the current limit on N from Planck is $50 \lesssim N \lesssim 60$ [109]. The equation of state parameter ω_ϕ for the fluid ϕ dominated after inflation should satisfy $|\Delta N| \lesssim 10$ using the uncertainties from CMB data.[5] The change in the number of e-folds due to nonstandard scenarios after inflation is [109–112]

$$\Delta N \approx \frac{1 - 3\omega_\phi}{12(1 + \omega_\phi)} \ln \frac{\rho_R(T_{\rm end})}{\rho_{\rm rh}}, \tag{4.4}$$

where $\rho_{\rm rh}$ is the total energy density after reheating. If the Universe is dominated by a scalar field (which could also be the inflaton itself), one has $\rho_{\rm rh} = M_\phi^2 \Delta\phi^2/2$, where M_ϕ corresponds to the mass of ϕ and $\Delta\phi \sim M_{\rm Pl}$ [110–112]. Using Eq. (3.8), Eq. (4.4) can be rewritten as

[5]The uncertainties in n_s and r related to the scale dependency of n_s can be written as [110–112]

$$\Delta n_s \approx (n_s - 1)\left[-\frac{5}{16}r - \frac{3}{64}\frac{r^2}{n_s - 1}\right]\Delta N, \tag{4.2}$$

$$\Delta r \approx r\left[n_s - 1 + \frac{r}{8}\right]\Delta N. \tag{4.3}$$

Using Planck data [109], previous equations impose a limit on ΔN given by $|\Delta N| \lesssim 10$.

$$\Delta N \approx \frac{1-3\omega_\phi}{12(1+\omega_\phi)}\left[-125.45+\ln\left[\left(\frac{g_\star(T_{\rm end})}{10.75}\right)\times\left(\frac{T_{\rm end}}{10\ {\rm MeV}}\right)^4\left(\frac{190\ {\rm TeV}}{M_\phi}\right)^2\left(\frac{M_{\rm Pl}}{\Delta\phi}\right)^2\right]\right], \tag{4.5}$$

where $\Gamma_\phi = M_\phi^3/(8\pi M_{\rm Pl}^2)$ was assumed. Typical values used in this work for ω_ϕ, $T_{\rm end}$ and Γ_ϕ agree with the CMB bound $|\Delta N| \lesssim 10$.

Moreover, nonstandard cosmological scenarios assuming different equations of state for ϕ can affect the growth of primordial density perturbations [113–115]. Primordial density perturbations for subhorizon modes ($k\tau \gg 1$) grow like $\delta\rho/\rho \propto a^{(3\omega_\phi-1)/2}$ for $\omega_\phi \neq 0$ and for $\omega_\phi = 0$ as $\delta\rho/\rho \propto a$ [113–116]. When the growth of perturbations is large, e.g. when it scales like a, it may boost the formation of large structures. However, these modes formed at temperatures higher than 1 MeV are much smaller than the size of horizon at the time of structure formation which happens at a temperature around 1 eV. Due to the diffusion (Silk) damping these modes are subdominant during the formation of structures and are not effective [116,117]. As a consequence, the nonstandard cosmologies we consider are by construction in agreement with the prediction of standard cosmology after BBN. Here we will generally focus on the nonstandard cosmological scenarios and their impacts on the PGW spectrum and their possible bounds from GW experiments.

The nonstandard cosmology can let an imprint for frequencies higher than

$$f_{\rm end} \equiv \frac{k_{\rm end}}{2\pi} = \frac{a_{\rm end}H_{\rm end}}{2\pi} \approx \frac{1}{6}\sqrt{\frac{g_\star(T_{\rm end})}{10}}\left[\frac{h_\star(T_0)}{h_\star(T_{\rm end})}\right]^{1/3} \times \frac{a_0 T_0 T_{\rm end}}{M_{\rm Pl}}, \tag{4.6}$$

where $H_{\rm end} \equiv H(T = T_{\rm end})$. Equation (4.6) is derived under assuming the entropy conservation for scale factors $a \gg a_{\rm end}$ until today. On the contrary, $f \ll f_{\rm end}$ corresponds to frequencies that cross the horizon after the end of the ϕ domination and therefore are not sensitive to the nonstandard phase. Similarly, the frequency $f_{\rm eq}$ corresponding to $a = a_{\rm eq}$ can be defined as

$$f_{\rm eq} \equiv \frac{k_{\rm eq}}{2\pi} \approx \frac{1}{6}\sqrt{\frac{g_\star(T_{\rm eq})}{5}}\left[\frac{h_\star(T_0)}{h_\star(T_{\rm dec})}\right]^{\frac{1}{3}} \times \left[\xi^{\frac{4}{3\omega_\phi-1}}\left(\left[\frac{g_\star(T_{\rm max})}{g_\star(T_{\rm dec})}\right]^{\frac{1}{4}}\frac{T_{\rm max}}{T_{\rm dec}}\right)^{3\omega_\phi-1}\right]^{\frac{1}{3(1+\omega_\phi)}}\frac{a_0 T_0 T_{\rm eq}^2}{M_{\rm Pl}T_{\rm max}}; \tag{4.7}$$

see the Appendix for details.

The present relic of gravitational waves can be approximately written as

$$\Omega_{\rm GW}(\eta_0, k) \approx \frac{\mathcal{P}_T(k)k^2 a_{\rm hc}^2}{24 a_0^4 H_0^2}, \tag{4.8}$$

where $a_{\rm hc}$ is the scale factor at horizon crossing and η_0 is the conformal time today. Considering a Universe dominated by a ϕ component before BBN leads to different regimes for the PGW spectrum depending on the moment where perturbations cross the horizon. We classify them in the following.

A. Classification

1. Case 1: $a_{\rm end} \ll a_{\rm hc}$

In this case perturbations cross the horizon well after the decay of ϕ, when $a_{\rm end} \ll a_{\rm hc}$. This corresponds to the standard scenario where the Universe is radiation dominated, and therefore the Hubble expansion rate scales like

$$H(a) = \sqrt{\frac{\rho_R(a)}{3M_{\rm Pl}^2}} = \tilde{H}_{\rm max}\left(\frac{a_{\rm start}}{a_{\rm end}}\right)^{\frac{3\omega_\phi-5}{4}}\left(\frac{a_{\rm max}}{a}\right)^2, \tag{4.9}$$

where

$$\tilde{H}_{\rm max} \equiv \frac{\pi}{3}\sqrt{\frac{g_\star(T_{\rm max})}{10}}\frac{T_{\rm max}^2}{M_{\rm Pl}} \tag{4.10}$$

corresponds to the contribution to H coming from the SM radiation at $T = T_{\rm max}$. Let us emphasize that $\tilde{H}_{\rm max} \neq H(T = T_{\rm max})$. Additionally, the scale factor $a_{\rm max}$ at $T_{\rm max}$ can be estimated to be

$$a_{\rm max} \approx a_0\frac{T_0}{T_{\rm max}}\left[\frac{h_\star(T_0)}{h_\star(T_{\rm dec})}\right]^{\frac{1}{3}} \times \left[\xi\left(\left[\frac{g_\star(T_{\rm max})}{g_\star(T_{\rm dec})}\right]^{\frac{1}{4}}\frac{T_{\rm max}}{T_{\rm dec}}\right)^{1-3\omega_\phi}\right]^{-\frac{1}{3(1+\omega_\phi)}}; \tag{4.11}$$

see the Appendix. Therefore, at the horizon crossing

$$k = a_{\rm hc}H(a_{\rm hc}) = \tilde{H}_{\rm max}\left(\frac{a_{\rm start}}{a_{\rm end}}\right)^{\frac{3\omega_\phi-5}{4}}\frac{a_{\rm max}^2}{a_{\rm hc}} \propto a_{\rm hc}^{-1}. \tag{4.12}$$

That dependence implies that $\Omega_{\rm GW}$ will inherit exactly the same scale dependence as the primordial spectrum

$$\Omega_{\rm GW}(\eta_0, k) \approx \frac{\mathcal{P}_T(k)}{24}\left(\frac{\tilde{H}_{\rm max}}{H_0}\right)^2\left(\frac{a_{\rm max}}{a_0}\right)^4\left(\frac{a_{\rm start}}{a_{\rm end}}\right)^{\frac{3\omega_\phi-5}{2}} \propto \mathcal{P}_T(k). \tag{4.13}$$

In particular, if the primordial spectrum is scale invariant, $\Omega_{\rm GW}$ becomes independent of k, up to changes in the relativistic degrees of freedom.

2. Case 2: $a_{\rm eq} \ll a_{\rm hc} \ll a_{\rm end}$

This case corresponds to the scenario where $a_{\rm eq} \ll a_{\rm hc} \ll a_{\rm end}$. Additionally, we demand that $\xi \gg \xi_{\rm min}$, which implies that a sizable relative increase of the temperature is achieved due to the decay of ϕ. This is typically realized when $\omega_\phi \ll 1/3$ and therefore $T_{\rm end} \approx T_{\rm dec}$. In this case ϕ dominates the Hubble expansion rate,[6] and therefore

$$\begin{aligned} H(a) &= \sqrt{\frac{\rho_\phi(a)}{3M_{\rm Pl}^2}} = \sqrt{\frac{\rho_\phi(a_{\rm max})}{3M_{\rm Pl}^2}}\left(\frac{a_{\rm max}}{a}\right)^{\frac{3}{2}(1+\omega_\phi)} \\ &= \frac{\pi}{3}\sqrt{\frac{g_\star(T_{\rm max})}{10}}\frac{T_{\rm max}^2}{M_{\rm Pl}}\sqrt{\xi}\left(\frac{a_{\rm max}}{a}\right)^{\frac{3}{2}(1+\omega_\phi)} \\ &= \tilde{H}_{\rm max}\sqrt{\xi}\left(\frac{a_{\rm max}}{a}\right)^{\frac{3}{2}(1+\omega_\phi)}. \end{aligned} \tag{4.14}$$

This implies that at the horizon crossing

$$k = a_{\rm hc}H(a_{\rm hc}) = \tilde{H}_{\rm max}\sqrt{\xi}a_{\rm max}^{\frac{3}{2}(1+\omega_\phi)}a_{\rm hc}^{-\frac{1+3\omega_\phi}{2}}. \tag{4.15}$$

That allows us to find an approximate expression for the present relic of a GW:

$$\Omega_{\rm GW}(\eta_0,k) \approx \frac{\mathcal{P}_T(k)}{24a_0^4H_0^2}\left[\tilde{H}_{\rm max}^2\xi a_{\rm max}^{3(1+\omega_\phi)}k^{3\omega_\phi-1}\right]^{\frac{2}{1+3\omega_\phi}}, \tag{4.16}$$

which presents an extra k dependence, additionally to the one from the primordial spectrum.

3. Case 3: $a_{\rm hc} \ll a_{\rm eq}$

This case corresponds to the scenario where $a_{\rm hc} \ll a_{\rm eq}$. We again demand that $\xi \gg \xi_{\rm min}$, which implies that a sizable relative increase of the temperature is achieved due to the decay of ϕ. This can only be realized when $\omega_\phi < 1/3$ and therefore $T_{\rm end} \approx T_{\rm dec}$. In this case the Universe is radiation dominated and then the Hubble rate evolves like

$$\begin{aligned} H(a) &= \sqrt{\frac{\rho_R(a)}{3M_{\rm Pl}^2}} = \sqrt{\frac{\rho_R(a_{\rm max})}{3M_{\rm Pl}^2}}\left(\frac{a_{\rm max}}{a}\right)^2 \\ &= \frac{\pi}{3}\sqrt{\frac{g_\star(T_{\rm max})}{10}}\frac{T_{\rm max}^2}{M_{\rm Pl}}\left(\frac{a_{\rm max}}{a}\right)^2 = \tilde{H}_{\rm max}\left(\frac{a_{\rm max}}{a}\right)^2. \end{aligned} \tag{4.17}$$

Here the horizon crossing happens for

$$k = a_{\rm hc}H(a_{\rm hc}) = \tilde{H}_{\rm max}\frac{a_{\rm max}^2}{a_{\rm hc}}. \tag{4.18}$$

Then the relic of PGW for radiation domination can be estimated to be

$$\Omega_{\rm GW}(\eta_0,k) \approx \frac{\mathcal{P}_T(k)}{24}\left(\frac{\tilde{H}_{\rm max}}{H_0}\right)^2\left(\frac{a_{\rm max}}{a_0}\right)^4, \tag{4.19}$$

where $a_{\rm max}$, given in Eq. (4.11), is the only place where a ξ dependence appears. As expected, Eq. (4.19) only depends on k via the primordial spectrum $\mathcal{P}_T(k)$.

4. Case 4: $\xi \ll \xi_{\rm min}$

This last case corresponds to the scenario where $\xi \ll \xi_{\rm min}$, which implies that either ρ_ϕ is subdominant when ϕ decays or that ϕ is not decaying at all. This is typically realized when $\omega_\phi \gg 1/3$.[7] Additionally, here $T_{\rm end} \gg T_{\rm dec}$. Let us also note that in this case $a_{\rm eq}$ and $a_{\rm start}$ are not defined, so the only relevant scale is $a = a_{\rm end}$. The scenario where $a_{\rm hc} \gg a_{\rm end}$ corresponds to the previously discussed case 1; now we focus on the opposite case $a_{\rm hc} \ll a_{\rm end}$.

In this scenario, as the energy density is dominated by ρ_ϕ, the Hubble expansion rate is given by Eq. (4.14). However, the scale factor $a_{\rm max}$ can now be computed by the use of the conservation of the SM entropy, which implies that

$$a_{\rm max} \approx a_0\frac{T_0}{T_{\rm max}}\left[\frac{h_\star(T_0)}{h_\star(T_{\rm max})}\right]^{\frac{1}{3}}, \tag{4.20}$$

which is now independent of ξ. Similar to case 1, the horizon crossing and the present relic of GW are given by Eqs. (4.15) and (4.16), respectively. Additionally, using Eq. (4.6) and entropy conservation, in this case[8]

$$\begin{aligned} f_{\rm end} &= \frac{a_{\rm end}H_{\rm end}}{2\pi} \\ &\approx \frac{1}{6}\left[\frac{h_\star(T_0)h_\star(T_{\rm max})}{h_\star(T_{\rm end})^2}\right]^{\frac{1}{3}}\sqrt{\frac{g_\star(T_{\rm end})}{10}}\xi^{\frac{1}{3\omega_\phi-1}}\frac{a_0T_0T_{\rm max}}{M_{\rm Pl}}. \end{aligned} \tag{4.21}$$

5. Scale-invariant primordial spectrum

Figure 3 shows examples of spectra of inflationary GWs. The upper panel corresponds to $\omega_\phi = 0$ and $\xi = 10^{-11}$, the central panel to $\omega_\phi = 1/3$ and $\xi = 10^{25}$ and the lower panel to $\omega_\phi = 2/3$ and $\xi = 10^{10}$. In all panels the temperature at

[6] Let us note that if $\omega_\phi > 1/3$, for $a < a_{\rm end}$ the Universe is always dominated by ϕ.

[7] In fact, for $\omega_\phi < 1/3$ and $\xi \ll \xi_{\rm min}$ the Universe is always radiation dominated and hence corresponds to the standard cosmology.

[8] Note that in this scenario $T_{\rm end} \approx T_{\rm max}\left[\frac{h_\star(T_{\rm max})}{h_\star(T_{\rm end})}\right]^{1/3}\xi^{\frac{1}{3\omega_\phi-1}}$.

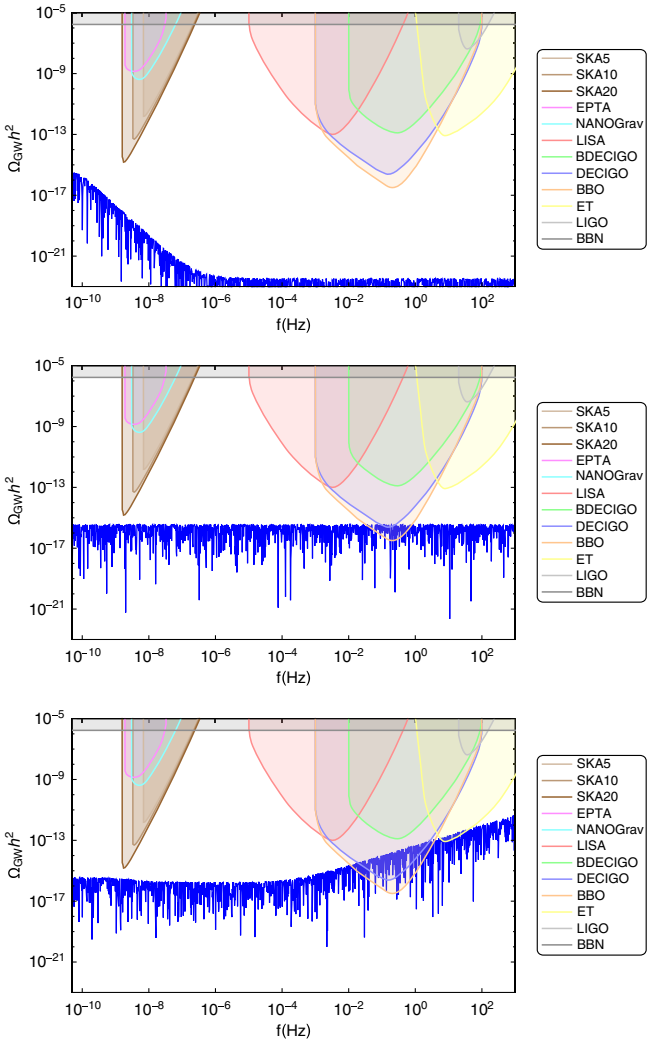

FIG. 3. Spectra of inflationary GWs for $\omega_\phi = 0$ and $\xi = 10^{-11}$ (upper panel), $\omega_\phi = 1/3$ and $\xi = 10^{25}$ (central panel), and $\omega_\phi = 2/3$ and $\xi = 10^{10}$ (lower panel). $T_{\rm dec} = 10$ MeV was also chosen. These benchmark points are the same used in Fig. 2 and are shown in the upper left panel of Fig. 4. The colored regions correspond to projected sensitivities for various gravitational wave observatories and to the BBN constraint described in the text.

which ϕ decays is assumed to be $T_{\rm dec} = 10$ MeV. Here we are considering a primordial scale-invariant spectrum ($n_T = 0$) with $V_{\rm inf}^{1/4} = 1.5 \times 10^{16}$ GeV. Let us note that the benchmarks are the same used in Fig. 2 and presented in the upper left panel of Fig. 4.

In the upper panel of Fig. 3 we assumed $\omega_\phi = 0$. For frequencies smaller than $f_{\rm end} \sim 10^{-10}$ Hz [Eq. (4.6)], perturbations crossed the horizon after the end of the ϕ domination and therefore are not sensitive to the nonstandard phase, case 1. The GW spectrum is therefore scale invariant, as the primordial spectrum. For higher frequencies, ϕ dominates the Hubble expansion rate and therefore $\Omega_{\rm GW} \propto f^{-2\frac{1-3\omega_\phi}{1+3\omega_\phi}} = f^{-2}$, case 2. For $f > f_{\rm eq} \sim 10^{-6}$ Hz [Eq. (4.7)], the Universe is again radiation dominated and therefore the spectrum becomes again scale invariant, case 3.

In the central panel of Fig. 3 we took $\omega_\phi = 1/3$, implying that the Universe is always dominated by a component that scales like radiation: either the SM radiation or ϕ. The GW spectrum has therefore the same k dependence as the primordial spectrum which is scale invariant.

Finally, in the lower panel of the figure $\omega_\phi = 2/3$ and $\xi < \xi_{\rm min}$. For $f < f_{\rm end} \sim 10^{-4}$ Hz [Eq. (4.21)], the GW spectrum is essentially flat, up to variations due to the change of the relativistic degrees of freedom. For $f > f_{\rm end}$, the GW spectrum is modified by the nonstandard phase and scales like $\Omega_{\rm GW} \propto f^{-2\frac{1-3\omega_\phi}{1+3\omega_\phi}} = f^{\frac{2}{3}}$, case 4.

Additionally, in Fig. 3 the colored regions correspond to projected sensitivities for various gravitational wave observatories [118]. In particular, we consider the proposed ground-based ET [9] and the planned space-based LISA [10] interferometer as well as the proposed successor experiments BBO [11] and (B-)DECIGO [12,13]. Moreover, we include pulsar timing arrays, in particular the currently operating European Pulsar Timing Array (EPTA) [119] and NANOGrav [120], as well as the future SKA [14] telescope. For the frequency range 10^{-3} to 10^2 Hz the $\Omega_{\rm GW}h^2 \sim 2 \times 10^{-17}$ is the lowest relic that can be probed by a BBO experiment. DECIGO can probe GW relics above $\sim 2 \times 10^{-16}$ in the same frequency range. Moreover, BDECIGO can probe frequencies between 10^{-2} and 10^2 Hz with a maximum sensitivity around 10^{-13}. A similar sensitivity could also be reached by LISA but in the frequency range 10^{-5} to 1 Hz. Very large frequencies between 1 and 10^4 Hz will be probed by the ET experiment for $\Omega_{\rm GW}h^2 \sim 2 \times 10^{-13}$. NANOGrav and EPTA can probe regions between 10^{-9} and 10^{-7} Hz with a relic above 10^{-9}. Finally, SKA can probe the regions between 10^{-9} and 10^{-6} Hz depending on the period of operation for 5, 10, and 20 years. The constraints from the LIGO/VIRGO Collaboration on the stochastic gravitational background and the coalescence of compact binary objects are also considered in our analysis [121,122]. A primordial gravitational wave relic as small as $\sim 3 \times 10^{-8}$ is not observed and therefore excluded for the frequency range between 10 and 200 Hz. Additionally, the PGW background as an extra radiation component modifies the expansion rate of Universe and can therefore be constrained by BBN [123]. This is done by using the measurement of the number of effective neutrinos $N_{\rm eff}$ and the observational abundance of D and ^{4}He, which impose $\Omega_{\rm GW}h^2 < \Omega_{\rm BBN}h^2 \simeq 1.7 \times 10^{-6}$ at 95% C.L. [124,125], which shows the integrated amount of PGW radiation. Combining the constraint from BBN on PGW background and Eq. (4.16) we can find the maximum frequency at which the Universe can start to be ϕ dominated:

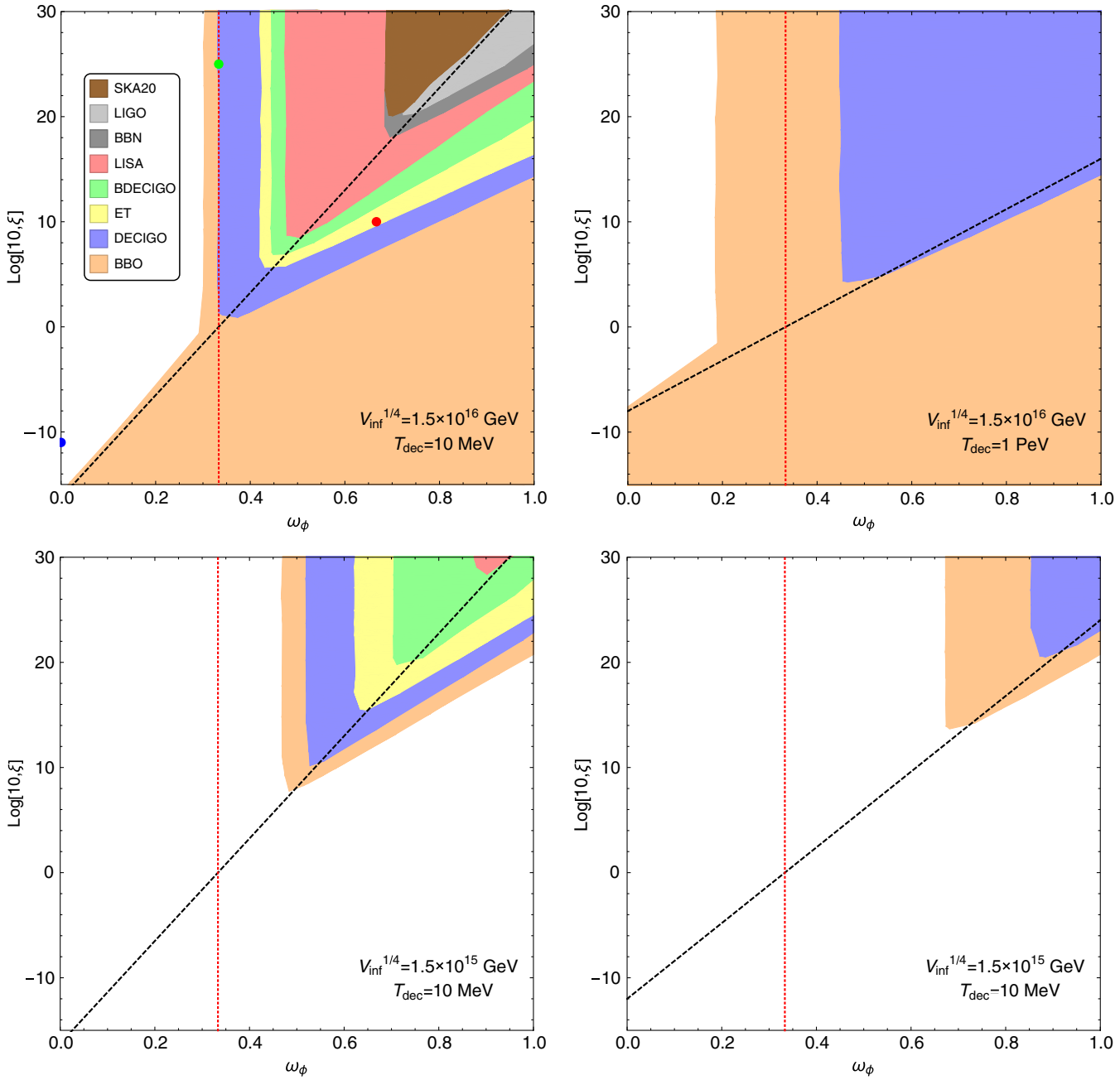

FIG. 4. Regions of the parameter space that could be tested by different observatories for a scale-invariant primordial spectrum ($n_T = 0$), taking $V_{\rm inf}^{1/4} = 1.5 \times 10^{16}$ (upper panels) and 1.5×10^{15} GeV (lower panels) and $T_{\rm dec} = 10$ MeV (left panels), 1 PeV (upper right panel) and 100 GeV (lower right panel). Three colored markers in the upper left panel are benchmark points for Figs. 2 and 3. The diagonal black dashed lines correspond to $\xi_{\rm min}$. The vertical red dotted lines correspond to $\omega_\phi = 1/3$.

$$k_{\rm BBN} \approx \left[\left(36\pi^2 \frac{a_0^4 M_{\rm Pl}^4 H_0^2 \Omega_{\rm BBN}}{V_{\rm inf}} \right)^{\frac{3\omega_\phi+1}{2}} \tilde{H}_{\rm max}^{-2} \xi^{-1} a_{\rm max}^{-3(1+\omega_\phi)} \right]^{\frac{1}{3\omega_\phi-1}}. \tag{4.22}$$

For frequencies larger than $f_{\rm BBN}$ the Universe should be either radiation dominated or during an inflationary phase. Other indirect possible constraints on PGW include the effect on temperature and polarization of the CMB and matter power spectra considered in Refs. [126,127]. However, these limits are not as competitive as the BBN bound.

Figure 4 shows in colors the regions of the parameter space $[\omega_\phi, \xi]$ that could be probed by different observatories for a scale-invariant primordial spectrum ($n_T = 0$), taking $V_{\rm inf}^{1/4} = 1.5 \times 10^{16}$ (upper panels) and 1.5×10^{15} GeV (lower panels) and $T_{\rm dec} = 10$ MeV (left panels), 1 PeV

(upper right panel) and 100 GeV (lower right panel). The lines correspond to $\xi = \xi_{\rm min}$ (black dashed lines) and $\omega_\phi = 1/3$ (red dotted vertical lines). Some general comments are in order. There is an important loss of sensitivity when decreasing the scale of inflation $V_{\rm inf}^{1/4}$, because the GW spectrum $\Omega_{\rm GW} \propto \mathcal{P}_T \propto V_{\rm inf}$. However, sensitivity increases when maximizing the ϕ-dominance period by decreasing $T_{\rm dec}$. One can see that different experiments could probe complementary regions of the parameter space, typically corresponding to equations of state $\omega_\phi > 1/3$ and to $\xi > \xi_{\rm min}$.

The behavior of the sensitivity regions can be understood as follows. Typically, the minimum value of equation of state parameter ω_ϕ that can be probed by a given experiment happens in case 2, when $a_{\rm eq} \ll a_{\rm hc} \ll a_{\rm end}$ and $\xi > \xi_{\rm min}$. It can be found by equaling $\Omega_{\rm GW}$ [Eq. (4.16)] with $\Omega_{\rm min}$, so that

$$\omega_{\phi,\rm min} \approx \frac{4}{3}\frac{\ln\left[\left(\frac{h_\star(T_0)}{h_\star(T_{\rm dec})}\right)^{\frac{1}{3}}\left(\frac{g_\star(T_{\rm dec})}{g_\star(T_{\rm max})}\right)^{\frac{1}{4}}\frac{a_0\tilde{H}_{\rm max}T_{\rm dec}T_0}{T_{\rm max}^2}\right]}{\ln\left[\left(\frac{h_\star(T_{\rm dec})}{h_\star(T_0)}\right)^{\frac{2}{3}}\left(\frac{g_\star(T_{\rm dec})}{g_\star(T_{\rm max})}\right)^{\frac{1}{2}}\frac{36\pi^2 a_0^2 M_{\rm Pl}^4 H_0^2 \Omega_{\rm min} T_{\rm dec}^2}{V_{\rm inf}k_{\rm min}^2 T_0^2}\right]} - \frac{1}{3}, \tag{4.23}$$

where $\Omega_{\rm min} \equiv \Omega_{\rm GW}(k_{\rm min})$ corresponds to the maximal sensitivity that a given experiment can reach and $k_{\rm min}$ to the wave number at which $\Omega_{\rm min}$ occurs. The fact that Eq. (4.23) is independent of ξ explains that the bounds on Fig. 4 appear as vertical lines.

However, the parameter space corresponding to $\omega_\phi < \omega_{\phi,\rm min}$ could also be probed. This corresponds to case 3, where $a_{\rm hc} \ll a_{\rm eq}$ and $\xi > \xi_{\rm min}$. The maximum ξ that can be probed by a given experiments can be derived from Eq. (4.19) to be

$$\xi \approx \left[\frac{g_\star(T_{\rm dec})T_{\rm dec}^4}{g_\star(T_{\rm max})T_{\rm max}^4}\right]\left[\left(\frac{h_\star(T_0)}{h_\star(T_{\rm dec})}\right)^{\frac{4}{3}}\frac{V_{\rm inf}}{36\pi^2\Omega_{\rm min}M_{\rm Pl}^4} \times \left(\frac{\tilde{H}_{\rm max}}{H_0}\right)^2\frac{T_0^4}{T_{\rm dec}^4}\frac{g_\star(T_{\rm max})}{g_\star(T_{\rm dec})}\right]^{\frac{3(1+\omega_\phi)}{4}} \tag{4.24}$$

and can be seen in the BBO bound for $\omega_\phi \lesssim 1/3$ in the two upper panels of Fig. 4.

Finally, the lower limit on ξ that can be explored with a GW observatory typically corresponds to case 4, where $\xi < \xi_{\rm min}$ and $\omega_\phi > \omega_{\phi,\rm min}$. In this scenario

$$\xi \approx \left[\frac{k_{\rm min}}{\tilde{H}_{\rm max}a_{\rm max}}\right]^2\left[\frac{36\pi^2 a_0^4 H_0^2 M_{\rm Pl}^4 \Omega_{\rm min}}{V_{\rm inf}k_{\rm min}^2 a_{\rm max}^2}\right]^{\frac{1+3\omega_\phi}{2}}, \tag{4.25}$$

which corresponds to the tilted colored lines for $\omega_\phi > 1/3$ in Fig. 4 and represents the typical minimum value of ξ that a given experiment can probe.

6. Effect of the tensor tilt

In the previous section the effect of nonstandard cosmologies on scale-invariant primordial spectra was studied. Here we generalize that analysis to spectra with nonzero tensor tilts [128]. The case of a primordial tensor power spectrum which is not scale invariant, having a k dependence is usually parameterized in the following manner [129]:

$$\mathcal{P}_T(k) = A_T\left(\frac{k}{\tilde{k}}\right)^{n_T}, \tag{4.26}$$

where $A_T = \frac{2}{3\pi^2}\frac{V_{\rm inf}}{M_{\rm Pl}^4}$ is the tensor amplitude at some pivot scale $\tilde{k}$ and n_T is the tensor spectral index. In general, A_T and n_T are independent parameters. However, in the single-field slow-roll scenario an interesting consistency relation holds between these quantities. The tensor-to-scalar ratio [7,130]

$$r \equiv \frac{A_T}{A_S} \tag{4.27}$$

yields the amplitude of the GW with respect to that of the scalar perturbations at some fixed pivot scale $\tilde{k}$, where $A_S \simeq 2.1 \times 10^{-9}$ [129] corresponds to the amplitude of primordial spectrum of curvature perturbations. At the lowest order in slow-roll parameters, the following consistency relation holds:

$$r = -8n_T. \tag{4.28}$$

For a radiation-dominated Universe before BBN and assuming the previous consistency relation, we scan over the parameter space of n_T and r to show the regions that could be constrained by GW experiments. Figure 5 shows the upper bounds on the parameter space of $[r, n_T]$ that can be probed by different GW experiments. The current BBN and LIGO bounds already constrain $n_T \gtrsim 0.5$ for $r \gtrsim 0.01$. The minimum value for the tensor tilt that can be probed by a given experiment can be approximated from Eqs. (2.13), (4.26) and (4.27) as

$$n_{T,\rm min} \approx \frac{\ln\left[\frac{48}{rA_S g_\star(T_{hc})}\frac{\Omega_{\rm min}}{\Omega_{\gamma,0}}\left[\frac{h_\star(T_{\rm hc})}{h_\star(T_0)}\right]^{4/3}\right]}{\ln\left[\frac{k_{\rm min}}{\tilde{k}}\right]}, \tag{4.29}$$

which has a logarithmic dependence on r. PGW observatories could probe large regions on the $[r, n_T]$ plane and eventually put constraints, stronger than the current CMB constraint limits [109].

Figure 6 depicts the regions of the parameter space that could be probed by different observatories assuming the consistency relation in Eq. (4.28) and $r = 0.07$, for $T_{\rm dec} = 10$ MeV (left panel) and 1 PeV (right panel).

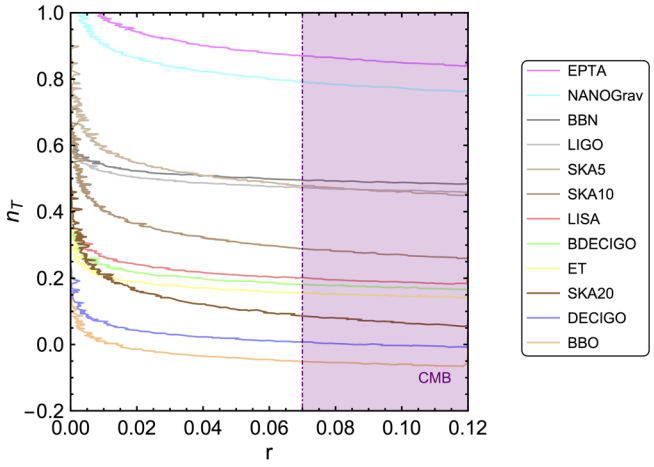

FIG. 5. Regions in the parameter space of the tensor-to-scalar ratio r and the tensor tilt n_T that can be probed by GW experiments in case of the standard radiation domination scenario. The regions above the colorful curves can be potentially excluded by different experiments. There are some comments in the right of plot in order, based on the minimum value of the tensor tilt that can be probed by each experiment. The dot-dashed purple line shows the upper bound on r from CMB by the *Planck* satellite [109].

However, the consistency relation may not hold. In Fig. 7 it is shown the regions of the parameter space that could be probed by different observatories assuming $n_T = -0.3$ (left panel) and $n_T = 0.3$ (right panel), for $T_{\rm dec} = 10$ MeV. The black dashed lines correspond to $\xi = \xi_{\rm min}$, the red dotted lines to $\omega_\phi = 1/3$.

The spectrum of PGW taking into account the possibility of a nonvanishing tensor tilt for modes which cross the horizon at scale factors in the range $a_{\rm eq} \ll a_{\rm hc} \ll a_{\rm end}$ (similar to case 2) can be estimated to be

$$\Omega_{\rm GW}(\eta_0, k) \approx \frac{A_T \tilde{H}_{\rm max}^{\frac{4}{1+3\omega_\phi}} \xi^{\frac{2}{1+3\omega_\phi}} a_{\rm max}^{\frac{6(1+\omega_\phi)}{1+3\omega_\phi}}}{24 a_0^4 H_0^2 \tilde{k}^{n_T}} k^{\frac{2(3\omega_\phi-1)}{1+3\omega_\phi}+n_T}. \quad (4.30)$$

The extra k^{n_T} dependence boosts (deteriorates) the detection prospects for the primordial GWs for $n_T > 0$ ($n_T < 0$), as shown in Figs. 6 and 7. In particular, the right panel of Fig. 7 shows a huge improvement on the detection possibilities in the case where $n_T = 0.3$.

As done in the previous section the typical minimum value of the equation of state parameter ω_ϕ that can be probed by a given experiment happens in case 2, when $a_{\rm eq} \ll a_{\rm hc} \ll a_{\rm end}$ and $\xi > \xi_{\rm min}$:

$$\omega_{\phi,\rm min} \approx \frac{4}{3} \frac{\ln\left[\left(\frac{h_\star(T_0)}{h_\star(T_{\rm dec})}\right)^{\frac{1}{3}} \left(\frac{g_\star(T_{\rm dec})}{g_\star(T_{\rm max})}\right)^{\frac{1}{4}} \frac{a_0 \tilde{H}_{\rm max} T_{\rm dec} T_0}{T_{\rm max}^2}\right]}{\ln\left[\left(\frac{h_\star(T_{\rm dec})}{h_\star(T_0)}\right)^{\frac{2}{3}} \left(\frac{g_\star(T_{\rm dec})}{g_\star(T_{\rm max})}\right)^{\frac{1}{2}} \frac{24 a_0^2 H_0^2 \Omega_{\rm min} T_{\rm dec}^2}{A_T k_{\rm min}^2 T_0^2} \left(\frac{\tilde{k}}{k_{\rm min}}\right)^{n_T}\right]} - \frac{1}{3}, \quad (4.31)$$

where $\Omega_{\rm min}$ is defined below Eq. (4.23). This relation matches with the minimum values of ω_ϕ obtained in Figs. 6 and 7 by precise numerical solutions, if one considers the numerical values for parameters and the values for $\Omega_{\rm min}$ and $k_{\rm min}$ from experimental constraints. These minima can take values smaller than $1/3$ due to the extra dependence of

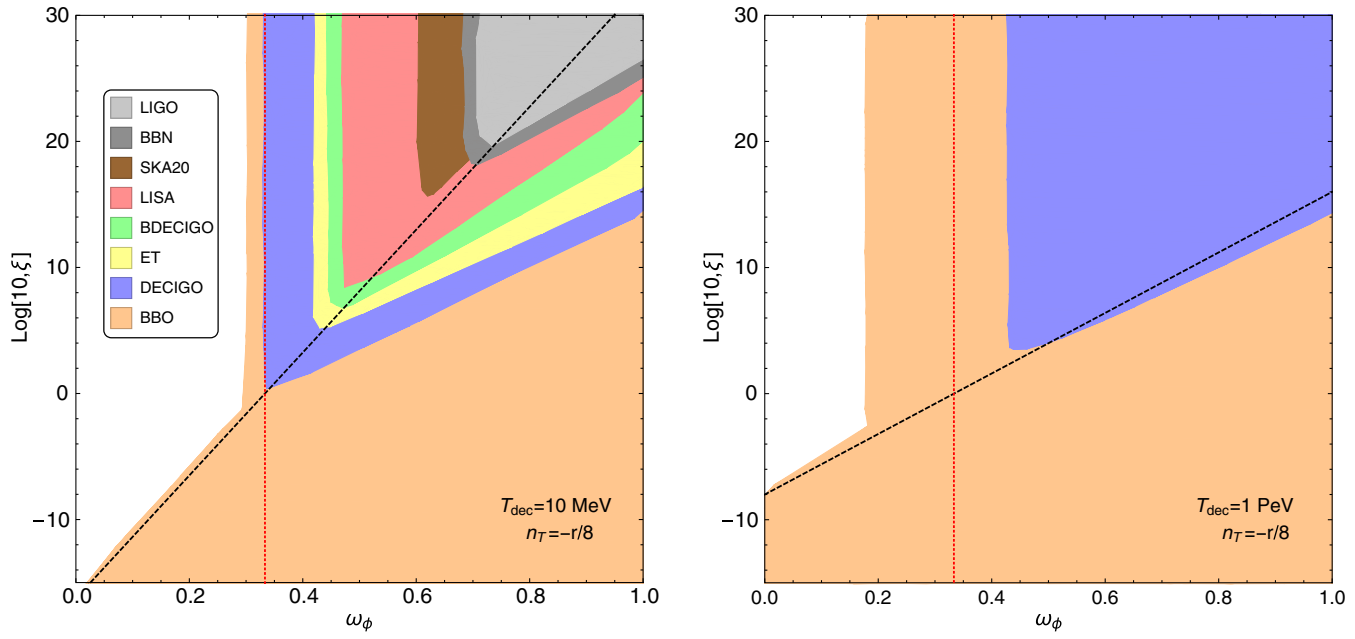

FIG. 6. Regions of the parameter space that could be tested by different observatories assuming the consistency relation, Eq. (4.28), and $r = 0.07$, for $T_{\rm dec} = 10$ MeV (left panel) and 1 PeV (right panel). The black dashed lines correspond to $\xi = \xi_{\rm min}$. The dotted red lines show the case $\omega_\phi = 1/3$.

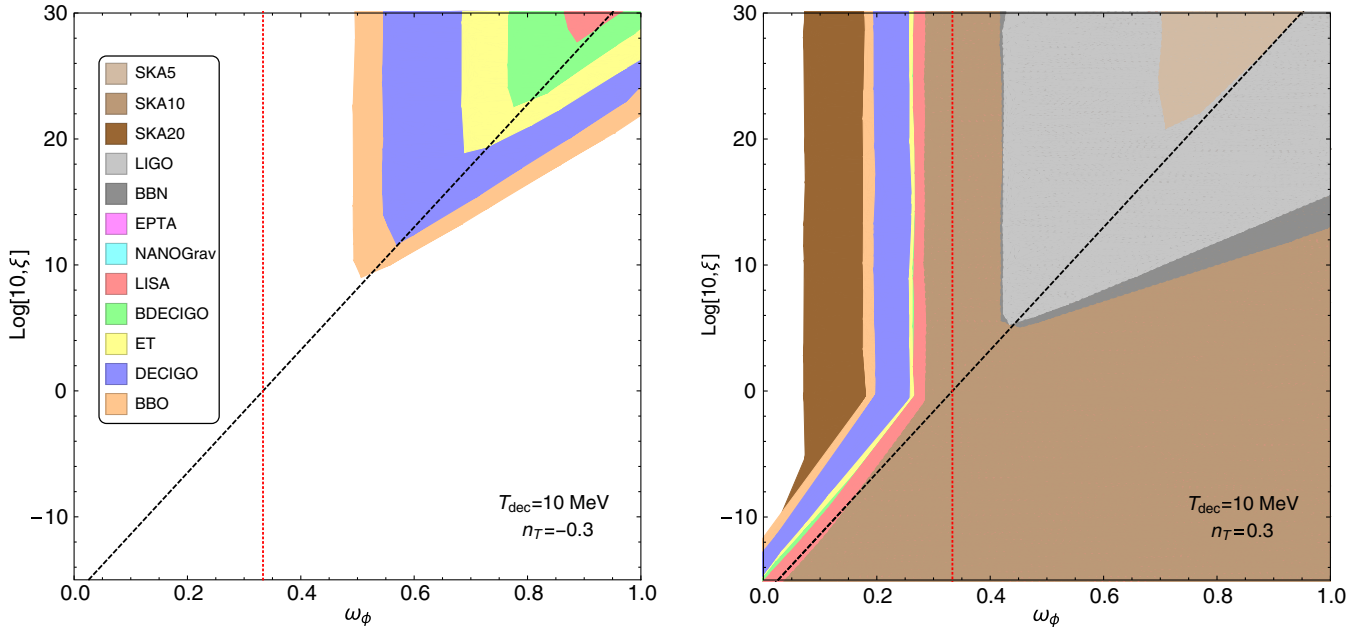

FIG. 7. Regions of the parameter space that could be tested by different observatories assuming $n_T = -0.3$ (left panel) and $n_T = 0.3$ (right panel), for $T_{\rm dec} = 10$ MeV. The black dashed lines correspond to $\xi = \xi_{\rm min}$. The red dotted lines show $\omega_\phi = 1/3$.

Eq. (4.31) on n_T, which shows some scenarios with a short period of early matter domination coming from small values of ξ and $n_T > 0$ that can be probed by future experiments.

In case 3, taking into account the tilt of the primordial spectrum, the maximum ξ then can be probed by a given experiment becomes

$$\xi \approx \left[\frac{g_\star(T_{\rm dec})T_{\rm dec}^4}{g_\star(T_{\rm max})T_{\rm max}^4}\right]\left[\left(\frac{h_\star(T_0)}{h_\star(T_{\rm dec})}\right)^{\frac{4}{3}}\frac{A_T}{24\Omega_{\rm min}}\left(\frac{k_{\rm min}}{\tilde{k}}\right)^{n_T} \times \left(\frac{\tilde{H}_{\rm max}}{H_0}\right)^2\frac{T_0^4}{T_{\rm dec}^4}\frac{g_\star(T_{\rm max})}{g_\star(T_{\rm dec})}\right]^{\frac{3(1+\omega_\phi)}{4}}. \quad (4.32)$$

Finally, the lower limit on ξ in case 4 becomes

$$\xi \approx \left[\frac{k_{\rm min}}{\tilde{H}_{\rm max}a_{\rm max}}\right]^2\left[24\frac{a_0^4H_0^2\Omega_{\rm min}}{A_T k_{\rm min}^2 a_{\rm max}^2}\left(\frac{\tilde{k}}{k_{\rm min}}\right)^{n_T}\right]^{\frac{1+3\omega_\phi}{2}}. \quad (4.33)$$

Equations (4.31)–(4.33) allow us to analytically understand the behaviors of the sensitivity curves in Figs. 6 and 7.

V. SUMMARY AND CONCLUSIONS

Inflation, as a well-motivated theory to explain the early Universe cosmological problems, predicts the existence of a PGW background. The spectrum of the inflationary GWs depends on the power spectrum of primordial tensor perturbations generated during inflation and the expansion rate of the Universe from the end of inflation until today. This stochastic GW background could be probed by different gravitational wave observatories. In this paper we studied the PGW spectrum in scenarios beyond the standard cosmological framework, where the evolution of the Universe is dominated by SM radiation. In fact, we analyzed nonstandard scenarios dominated by a long-lived component with a general equation of state. These cases are common in several UV-complete beyond the SM theories.

First we revisited the PGW spectrum in the case of a standard cosmology (i.e. with an energy density dominated by SM radiation), taking particular care of the evolution of the relativistic degrees of freedom, Fig. 1. Then we present the formalism used in order to define the nonstandard cosmology. We assume that for some period in the early Universe, the total energy density was dominated by a component ϕ with a general equation of state parameter ω_ϕ. We also assume that this component decays solely into SM radiation. In addition to ω_ϕ, the nonstandard cosmology was parameterized by the ratio ξ of ϕ to SM radiation energy densities and the temperature $T_{\rm end}$ at which ϕ decays. This framework completely fixes the evolution of the energy densities, the Hubble expansion rate of the Universe and the evolution of the photon temperature and allows us to numerically track in detail their behavior, Fig. 2.

In Sec. IV, PGWs in nonstandard cosmologies were studied. In particular, in Sec. 4. 1 we have analyzed the different possibilities and phenomenological consequences in which nonstandard cosmologies can impact the PGW spectrum. This strongly depends on the moment where the perturbations cross the horizon, with respect to the different characteristic scales $a_{\rm eq}$, $a_{\rm start}$ and $a_{\rm end}$. These analytical results were confronted and validated with numerical computations, e.g. Fig. 3.

Once a signal from a PGW is found, GW experiments can start probing the equation of state of the early Universe, in a given inflationary scenario. Using the projected limits from

future GW detectors, we study the possibilities to probe the parameter space $[\omega_\phi, \xi]$ in Fig. 4. We explore the impact of varying the scale of inflation and the temperature at which ϕ decays in the case where the primordial GW spectrum is scale invariant. The general case where the primordial GW spectrum has a scale dependence was also analyzed and the results were shown in Figs. 6 (assuming the single-field slow-roll consistency relation) and 7 (general case). Additionally, we scanned over the parameter space $[r, n_T]$ in Fig. 5 to find the minimum value of the scalar-to-tensor ratio that different GW experiments can probe.

ACKNOWLEDGMENTS

We would like to thank Juan Pablo Beltrán-Almeida, Mohammad Ali Gorji, Toby Opferkuch, Javier Rubio, Ken'ichi Saikawa, Jürgen Schaffner-Bielich and Dominik Schwarz for valuable discussions. N. B. is partially supported by Spanish MINECO under Grant No. FPA2017-84543-P. F. H. is supported by the Deutsche Forschungsgemeinschaft (DFG, German Research Foundation), Project No. 315477589, TRR 211. This project has received funding from the European Union's Horizon 2020 research and innovation program under the Marie Sklodowska-Curie Grant Agreements No. 674896 and No. 690575 and from Universidad Antonio Nariño Grants No. 2017239 and No. 2018204.

APPENDIX: SUDDEN DECAY APPROXIMATION OF ϕ

From Eq. (3.11) one has that the temperature scales like

$$\left[\frac{g_\star(T_{\rm max})}{g_\star(T_{\rm start})}\right]^{\frac{1}{4}}\frac{T_{\rm max}}{T_{\rm start}} = \frac{a_{\rm start}}{a_{\rm max}}, \tag{A1}$$

$$\left[\frac{g_\star(T_{\rm dec})}{g_\star(T_{\rm start})}\right]^{\frac{1}{4}}\frac{T_{\rm dec}}{T_{\rm start}} = \left(\frac{a_{\rm start}}{a_{\rm dec}}\right)^{\frac{3}{8}(1+\omega_\phi)}, \tag{A2}$$

$$\left[\frac{h_\star(T_{\rm dec})}{h_\star(T_0)}\right]^{\frac{1}{3}}\frac{T_{\rm dec}}{T_0} = \frac{a_0}{a_{\rm dec}}. \tag{A3}$$

Additionally, in the sudden decay approximation of ϕ, the conservation of energy density implies

$$\rho_R(T_1) + \rho_\phi(T_1) = \rho_R(T_2), \tag{A4}$$

and therefore

$$g_\star(T_1)T_1^4 + \xi g_\star(T_{\rm max})T_{\rm max}^4\left[\left(\frac{g_\star(T_1)}{g_\star(T_{\rm max})}\right)^{\frac{1}{4}}\frac{T_1}{T_{\rm max}}\right]^{3(1+\omega_\phi)} = g_\star(T_2)T_2^4, \tag{A5}$$

$$g_\star(T_1)^{1/4}T_1 = \left[\frac{1}{\xi}(g_\star(T_2)T_2^4)(g_\star(T_{\rm max})^{1/4}T_{\rm max})^{3\omega_\phi-1}\right]^{\frac{1}{3(1+\omega_\phi)}}, \tag{A6}$$

where T_1 and T_2 are the temperatures just before and just after ϕ decays, respectively. Taking into account the scaling of ρ_ϕ and that $\rho_\phi(T_{\rm max}) = \xi\rho_R(T_{\rm max})$, one gets that

$$\left[\frac{g_\star(T_2)}{g_\star(T_1)}\right]^{\frac{1}{4}}\frac{T_2}{T_1} = \left[\frac{g_\star(T_{\rm dec})}{g_\star(T_{\rm max})}\right]^{\frac{1}{4}}\frac{T_{\rm dec}}{T_{\rm max}}\frac{a_{\rm dec}}{a_{\rm max}} = \left[\xi\left(\left[\frac{g_\star(T_2)}{g_\star(T_{\rm max})}\right]^{\frac{1}{4}}\frac{T_2}{T_{\rm max}}\right)^{3\omega_\phi-1}\right]^{\frac{1}{3(1+\omega_\phi)}}. \tag{A7}$$

In this approximation, T_2 can be identified with $T_{\rm dec}$. Equations (A1), (A2) and (A7) can be rewritten, respectively, as

$$a_{\rm dec} = a_{\rm max}\left[\frac{g_\star(T_{\rm max})}{g_\star(T_{\rm dec})}\right]^{\frac{1}{4}} \times \frac{T_{\rm max}}{T_{\rm dec}}\left[\xi\left(\left[\frac{g_\star(T_{\rm max})}{g_\star(T_{\rm dec})}\right]^{\frac{1}{4}}\frac{T_{\rm max}}{T_{\rm dec}}\right)^{1-3\omega_\phi}\right]^{\frac{1}{3(1+\omega_\phi)}}, \tag{A8}$$

$$T_{\rm start} = T_{\rm dec}\left[\frac{g_\star(T_{\rm dec})}{g_\star(T_{\rm start})}\right]^{\frac{1}{4}}\left[\xi\left(\left[\frac{g_\star(T_{\rm max})}{g_\star(T_{\rm dec})}\right]^{\frac{1}{4}}\frac{T_{\rm max}}{T_{\rm dec}}\right)^{1-3\omega_\phi}\right]^{\frac{1}{5-3\omega_\phi}}, \tag{A9}$$

$$a_{\rm start} = a_{\rm max}\xi^{\frac{1}{3\omega_\phi-5}}\left[\left(\frac{g_\star(T_{\rm max})}{g_\star(T_{\rm dec})}\right)^{\frac{1}{4}}\frac{T_{\rm max}}{T_{\rm dec}}\right]^{\frac{4}{5-3\omega_\phi}}. \tag{A10}$$

Additionally, the equality $\rho_R = \rho_\phi$ happens at

$$T_{\rm eq} = \left[\frac{g_\star(T_{\rm max})}{g_\star(T_{\rm eq})}\right]^{\frac{1}{4}}T_{\rm max}\xi^{\frac{1}{1-3\omega_\phi}}, \tag{A11}$$

$$a_{\rm eq} = a_{\rm max}\xi^{\frac{1}{3\omega_\phi-1}}. \tag{A12}$$

Moreover, $a_{\rm max}$ can be extracted from Eqs. (A3) and (A8) and has the form of Eq. (4.11).

Finally, assuming $T_1, T_2 \to T_{\rm dec}$ and using Eq. (A6), the minimum value of ξ that leads to a ϕ domination phase which affects the evolution of radiation energy density can be obtained as

$$\xi_{\rm min} \approx \left[\left(\frac{g_\star(T_{\rm max})}{g_\star(T_{\rm dec})}\right)^{\frac{1}{4}}\frac{T_{\rm max}}{T_{\rm dec}}\right]^{3\omega_\phi-1}. \tag{A13}$$

If $\xi \gg \xi_{\rm min}$, ϕ dominates for some period the expansion rate of the Universe and also modifies the radiation energy density as $\rho_R \sim a^{-\frac{3}{2}(1+\omega_\phi)}$ until $T_{\rm end} \approx T_{\rm dec}$. In the opposite case, if $\xi \ll \xi_{\rm min}$ for $\omega_\phi < 1/3$, the ϕ domination regime never happens. However, for $\omega_\phi > 1/3$ if $1 < \xi \ll \xi_{\rm min}$, the Universe is dominated by ϕ but the radiation energy density is not significantly modified by the presence of ϕ.

[1] LIGO Scientific and Virgo Collaborations, Observation of Gravitational Waves from a Binary Black Hole Merger, Phys. Rev. Lett. **116**, 061102 (2016).

[2] LIGO Scientific and Virgo Collaborations, GW151226: Observation of Gravitational Waves from a 22-Solar-Mass Binary Black Hole Coalescence, Phys. Rev. Lett. **116**, 241103 (2016).

[3] LIGO Scientific and Virgo Collaborations, GW170104: Observation of a 50-Solar-Mass Binary Black Hole Coalescence at Redshift 0.2, Phys. Rev. Lett. **118**, 221101 (2017).

[4] LIGO Scientific and Virgo Collaborations, GW170814: A Three-Detector Observation of Gravitational Waves from a Binary Black Hole Coalescence, Phys. Rev. Lett. **119**, 141101 (2017).

[5] LIGO Scientific and Virgo Collaborations, GW170817: Observation of Gravitational Waves from a Binary Neutron Star Inspiral, Phys. Rev. Lett. **119**, 161101 (2017).

[6] LIGO Scientific and Virgo Collaborations, GW170608: Observation of a 19-solar-mass binary black hole coalescence, Astrophys. J. **851**, L35 (2017).

[7] M. C. Guzzetti, N. Bartolo, M. Liguori, and S. Matarrese, Gravitational waves from inflation, Riv. Nuovo Cimento **39**, 399 (2016).

[8] C. Caprini and D. G. Figueroa, Cosmological backgrounds of gravitational waves, Classical Quantum Gravity **35**, 163001 (2018).

[9] B. Sathyaprakash *et al.*, Scientific objectives of Einstein telescope, Classical Quantum Gravity **29**, 124013 (2012).

[10] LISA Collaboration, Laser interferometer space antenna, arXiv:1702.00786.

[11] J. Crowder and N. J. Cornish, Beyond LISA: Exploring future gravitational wave missions, Phys. Rev. D **72**, 083005 (2005).

[12] N. Seto, S. Kawamura, and T. Nakamura, Possibility of Direct Measurement of the Acceleration of the Universe Using 0.1-Hz Band Laser Interferometer Gravitational Wave Antenna in Space, Phys. Rev. Lett. **87**, 221103 (2001).

[13] S. Sato *et al.*, The status of DECIGO, J. Phys. Conf. Ser. **840**, 012010 (2017).

[14] G. Janssen *et al.*, Gravitational wave astronomy with the SKA, Proc. Sci., AASKA14 (**2015**) 037.

[15] L. P. Grishchuk, Amplification of gravitational waves in an istropic universe, Sov. Phys. JETP **40**, 409 (1975).

[16] A. A. Starobinsky, Spectrum of relict gravitational radiation and the early state of the universe, JETP Lett. **30**, 682 (1979).

[17] S. Kuroyanagi, T. Chiba, and T. Takahashi, Probing the universe through the stochastic gravitational wave background, J. Cosmol. Astropart. Phys. 11 (2018) 038.

[18] COrE Collaboration, COrE (Cosmic Origins Explorer) A white paper, arXiv:1102.2181.

[19] G. Cabass, L. Pagano, L. Salvati, M. Gerbino, E. Giusarma, and A. Melchiorri, Updated constraints and forecasts on primordial tensor modes, Phys. Rev. D **93**, 063508 (2016).

[20] E. T. Vishniac, Relativistic collisionless particles and the evolution of cosmological perturbations, Astrophys. J. **257**, 456 (1982).

[21] A. K. Rebhan and D. J. Schwarz, Kinetic versus thermal field theory approach to cosmological perturbations, Phys. Rev. D **50**, 2541 (1994).

[22] D. J. Schwarz, Evolution of gravitational waves through cosmological transitions, Mod. Phys. Lett. A **13**, 2771 (1998).

[23] N. Seto and J. Yokoyama, Probing the equation of state of the early universe with a space laser interferometer, J. Phys. Soc. Jpn. **72**, 3082 (2003).

[24] S. Weinberg, Damping of tensor modes in cosmology, Phys. Rev. D **69**, 023503 (2004).

[25] S. Bashinsky, Coupled evolution of primordial gravity waves and relic neutrinos, arXiv:astro-ph/0505502.

[26] D. A. Dicus and W. W. Repko, Comment on damping of tensor modes in cosmology, Phys. Rev. D **72**, 088302 (2005).

[27] L. A. Boyle and P. J. Steinhardt, Probing the early universe with inflationary gravitational waves, Phys. Rev. D **77**, 063504 (2008).

[28] Y. Watanabe and E. Komatsu, Improved calculation of the primordial gravitational wave spectrum in the Standard Model, Phys. Rev. D **73**, 123515 (2006).

[29] S. Kuroyanagi, T. Chiba, and N. Sugiyama, Precision calculations of the gravitational wave background spectrum from inflation, Phys. Rev. D **79**, 103501 (2009).

[30] A. Mangilli, N. Bartolo, S. Matarrese, and A. Riotto, The impact of cosmic neutrinos on the gravitational-wave background, Phys. Rev. D **78**, 083517 (2008).

[31] B. A. Stefanek and W. W. Repko, Analytic description of the damping of gravitational waves by free streaming neutrinos, Phys. Rev. D **88**, 083536 (2013).

[32] J. B. Dent, L. M. Krauss, S. Sabharwal, and T. Vachaspati, Damping of primordial gravitational waves from generalized sources, Phys. Rev. D **88**, 084008 (2013).

[33] G. Baym, S. P. Patil, and C. J. Pethick, Damping of gravitational waves by matter, Phys. Rev. D **96**, 084033 (2017).

[34] R. R. Caldwell, T. L. Smith, and D. G. E. Walker, Using a primordial gravitational wave background to illuminate new physics, Phys. Rev. D **100**, 043513 (2019).

[35] S. Davidson, M. Losada, and A. Riotto, A New Perspective on Baryogenesis, Phys. Rev. Lett. **84**, 4284 (2000).

[36] G. F. Giudice, E. W. Kolb, and A. Riotto, Largest temperature of the radiation era and its cosmological implications, Phys. Rev. D **64**, 023508 (2001).

[37] R. Allahverdi, B. Dutta, and K. Sinha, Baryogenesis and late-decaying moduli, Phys. Rev. D **82**, 035004 (2010).

[38] A. Beniwal, M. Lewicki, J. D. Wells, M. White, and A. G. Williams, Gravitational wave, collider and dark matter signals from a scalar singlet electroweak baryogenesis, J. High Energy Phys. 08 (2017) 108.

[39] R. Allahverdi, P. S. B. Dev, and B. Dutta, A simple testable model of baryon number violation: Baryogenesis, dark matter, neutron–antineutron oscillation and collider signals, Phys. Lett. B **779**, 262 (2018).

[40] B. Dutta, C. S. Fong, E. Jimenez, and E. Nardi, A cosmological pathway to testable leptogenesis, J. Cosmol. Astropart. Phys. 10 (2018) 025.

[41] N. Bernal and C. S. Fong, Hot leptogenesis from thermal dark matter, J. Cosmol. Astropart. Phys. 10 (2017) 042.

[42] H. Assadullahi and D. Wands, Gravitational waves from an early matter era, Phys. Rev. D **79**, 083511 (2009).
[43] R. Durrer and J. Hasenkamp, Testing superstring theories with gravitational waves, Phys. Rev. D **84**, 064027 (2011).
[44] L. Alabidi, K. Kohri, M. Sasaki, and Y. Sendouda, Observable induced gravitational waves from an early matter phase, J. Cosmol. Astropart. Phys. 05 (2013) 033.
[45] F. D'Eramo and K. Schmitz, Imprint of a scalar era on the primordial spectrum of gravitational waves, arXiv:1904.07870.
[46] K. Inomata, K. Kohri, T. Nakama, and T. Terada, Gravitational waves induced by scalar perturbations during a gradual transition from an early matter era to the radiation era, arXiv:1904.12878.
[47] K. Inomata, K. Kohri, T. Nakama, and T. Terada, Enhancement of gravitational waves induced by scalar perturbations due to a sudden transition from an early matter era to the radiation era, arXiv:1904.12879.
[48] M. Kamionkowski and M. S. Turner, Thermal relics: Do we know their abundances, Phys. Rev. D **42**, 3310 (1990).
[49] P. Salati, Quintessence and the relic density of neutralinos, Phys. Lett. B **571**, 121 (2003).
[50] D. Comelli, M. Pietroni, and A. Riotto, Dark energy and dark matter, Phys. Lett. B **571**, 115 (2003).
[51] F. Rosati, Quintessential enhancement of dark matter abundance, Phys. Lett. B **570**, 5 (2003).
[52] G. B. Gelmini and P. Gondolo, Neutralino with the right cold dark matter abundance in (almost) any supersymmetric model, Phys. Rev. D **74**, 023510 (2006).
[53] G. Gelmini, P. Gondolo, A. Soldatenko, and C. E. Yaguna, The effect of a late decaying scalar on the neutralino relic density, Phys. Rev. D **74**, 083514 (2006).
[54] A. Arbey and F. Mahmoudi, SUSY constraints from relic density: High sensitivity to pre-BBN expansion rate, Phys. Lett. B **669**, 46 (2008).
[55] G. B. Gelmini and P. Gondolo, Ultra-cold WIMPs: Relics of non-standard pre-BBN cosmologies, J. Cosmol. Astropart. Phys. 10 (2008) 002.
[56] A. Arbey and F. Mahmoudi, SUSY constraints, relic density, and very early universe, J. High Energy Phys. 05 (2010) 051.
[57] L. Visinelli and P. Gondolo, Axion cold dark matter in nonstandard cosmologies, Phys. Rev. D **81**, 063508 (2010).
[58] R. T. Co, F. D'Eramo, L. J. Hall, and D. Pappadopulo, Freeze-in dark matter with displaced signatures at colliders, J. Cosmol. Astropart. Phys. 12 (2015) 024.
[59] A. Berlin, D. Hooper, and G. Krnjaic, PeV-scale dark matter as a thermal relic of a decoupled sector, Phys. Lett. B **760**, 106 (2016).
[60] T. Tenkanen and V. Vaskonen, Reheating the Standard Model from a hidden sector, Phys. Rev. D **94**, 083516 (2016).
[61] J. A. Dror, E. Kuflik, and W. H. Ng, Codecaying Dark Matter, Phys. Rev. Lett. **117**, 211801 (2016).
[62] A. Berlin, D. Hooper, and G. Krnjaic, Thermal dark matter from a highly decoupled sector, Phys. Rev. D **94**, 095019 (2016).
[63] B. Dutta, E. Jimenez, and I. Zavala, Dark matter relics and the expansion rate in scalar-tensor theories, J. Cosmol. Astropart. Phys. 06 (2017) 032.
[64] F. D'Eramo, N. Fernandez, and S. Profumo, When the universe expands too fast: Relentless dark matter, J. Cosmol. Astropart. Phys. 05 (2017) 012.
[65] S. Hamdan and J. Unwin, Dark matter freeze-out during matter domination, Mod. Phys. Lett. A **33**, 1850181 (2018).
[66] L. Visinelli, (Non-)thermal production of WIMPs during kination, Symmetry **10**, 546 (2018).
[67] J. A. Dror, E. Kuflik, B. Melcher, and S. Watson, Concentrated dark matter: Enhanced small-scale structure from codecaying dark matter, Phys. Rev. D **97**, 063524 (2018).
[68] M. Drees and F. Hajkarim, Dark matter production in an early matter dominated era, J. Cosmol. Astropart. Phys. 02 (2018) 057.
[69] F. D'Eramo, N. Fernandez, and S. Profumo, Dark matter freeze-in production in fast-expanding universes, J. Cosmol. Astropart. Phys. 02 (2018) 046.
[70] N. Bernal, C. Cosme, and T. Tenkanen, Phenomenology of self-interacting dark matter in a matter-dominated universe, Eur. Phys. J. C **79**, 99 (2019).
[71] E. Hardy, Higgs portal dark matter in non-standard cosmological histories, J. High Energy Phys. 06 (2018) 043.
[72] D. Maity and P. Saha, CMB constraints on dark matter phenomenology via reheating in Minimal plateau inflation, Phys. Dark Universe **25**, 100317 (2019).
[73] T. Hambye, A. Strumia, and D. Teresi, Super-cool dark matter, J. High Energy Phys. 08 (2018) 188.
[74] N. Bernal, C. Cosme, T. Tenkanen, and V. Vaskonen, Scalar singlet dark matter in non-standard cosmologies, Eur. Phys. J. C **79**, 30 (2019).
[75] A. Arbey, J. Ellis, F. Mahmoudi, and G. Robbins, Dark matter casts light on the early universe, J. High Energy Phys. 10 (2018) 132.
[76] A. E. Nelson and H. Xiao, Axion cosmology with early matter domination, Phys. Rev. D **98**, 063516 (2018).
[77] M. Drees and F. Hajkarim, Neutralino dark matter in scenarios with early matter domination, J. High Energy Phys. 12 (2018) 042.
[78] A. Betancur and Ó. Zapata, Phenomenology of doublet-triplet fermionic dark matter in nonstandard cosmology and multicomponent dark sectors, Phys. Rev. D **98**, 095003 (2018).
[79] E. V. Arbuzova, A. D. Dolgov, and R. S. Singh, Dark matter in $R + R^2$ cosmology, J. Cosmol. Astropart. Phys. 04 (2019) 014.
[80] C. Maldonado and J. Unwin, Establishing the dark matter relic density in an era of particle decays, J. Cosmol. Astropart. Phys. 06 (2019) 037.
[81] P. Arias, N. Bernal, A. Herrera, and C. Maldonado, Reconstructing non-standard cosmologies with dark matter, arXiv:1906.04183.
[82] L. Heurtier and F. Huang, The inflaton portal to a highly decoupled EeV dark matter particle, Phys. Rev. D **100**, 043507 (2019).
[83] D. Maity and P. Saha, Connecting CMB anisotropy and cold dark matter phenomenology via reheating, Phys. Rev. D **98**, 103525 (2018).
[84] V. Sahni, The energy density of relic gravity waves from inflation, Phys. Rev. D **42**, 453 (1990).

[85] M. Giovannini, Gravitational waves constraints on post-inflationary phases stiffer than radiation, Phys. Rev. D **58**, 083504 (1998).
[86] M. Giovannini, Production and detection of relic gravitons in quintessential inflationary models, Phys. Rev. D **60**, 123511 (1999).
[87] A. Riazuelo and J.-P. Uzan, Quintessence and gravitational waves, Phys. Rev. D **62**, 083506 (2000).
[88] V. Sahni, M. Sami, and T. Souradeep, Relic gravity waves from brane world inflation, Phys. Rev. D **65**, 023518 (2001).
[89] H. Tashiro, T. Chiba, and M. Sasaki, Reheating after quintessential inflation and gravitational waves, Classical Quantum Gravity **21**, 1761 (2004).
[90] K. Saikawa and S. Shirai, Primordial gravitational waves, precisely: The role of thermodynamics in the Standard Model, J. Cosmol. Astropart. Phys. 05 (2018) 035.
[91] N. Ramberg and L. Visinelli, Probing the Early Universe with Axion Physics and Gravitational Waves, Phys. Rev. D **99**, 123513 (2019).
[92] T. Opferkuch, P. Schwaller, and B. A. Stefanek, Ricci Reheating, J. Cosmol. Astropart. Phys. 07 (2019) 016.
[93] K. D. Lozanov and M. A. Amin, Self-resonance after inflation: Oscillons, transients and radiation domination, Phys. Rev. D **97**, 023533 (2018).
[94] K. D. Lozanov and M. A. Amin, Equation of State and Duration to Radiation Domination after Inflation, Phys. Rev. Lett. **119**, 061301 (2017).
[95] R. C. Nunes, M. E. S. Alves, and J. C. N. de Araujo, Primordial gravitational waves in Horndeski gravity, Phys. Rev. D **99**, 084022 (2019).
[96] Y. Cui, M. Lewicki, D. E. Morrissey, and J. D. Wells, Cosmic archaeology with gravitational waves from cosmic strings, Phys. Rev. D **97**, 123505 (2018).
[97] Y. Cui, M. Lewicki, D. E. Morrissey, and J. D. Wells, Probing the pre-BBN universe with gravitational waves from cosmic strings, J. High Energy Phys. 01 (2019) 081.
[98] M. Artymowski, O. Czerwińska, Z. Lalak, and M. Lewicki, Gravitational wave signals and cosmological consequences of gravitational reheating, J. Cosmol. Astropart. Phys. 04 (2018) 046.
[99] M. Scomparin and S. Vazzoler, Damping of cosmological tensor modes in Horndeski theories after GW170817, arXiv:1903.01502.
[100] A. R. Liddle, The Inflationary energy scale, Phys. Rev. D **49**, 739 (1994).
[101] M. Drees, F. Hajkarim, and E. R. Schmitz, The effects of QCD equation of state on the relic density of WIMP dark matter, J. Cosmol. Astropart. Phys. 06 (2015) 025.
[102] S. Schettler, T. Boeckel, and J. Schaffner-Bielich, Imprints of the QCD phase transition on the spectrum of gravitational waves, Phys. Rev. D **83**, 064030 (2011).
[103] F. Hajkarim, J. Schaffner-Bielich, S. Wystub, and M. M. Wygas, Effects of the QCD equation of state and lepton asymmetry on primordial gravitational waves, Phys. Rev. D **99**, 103527 (2019).
[104] M. Kawasaki, K. Kohri, and N. Sugiyama, MeV scale reheating temperature and thermalization of neutrino background, Phys. Rev. D **62**, 023506 (2000).
[105] S. Hannestad, What is the lowest possible reheating temperature, Phys. Rev. D **70**, 043506 (2004).
[106] K. Ichikawa, M. Kawasaki, and F. Takahashi, The oscillation effects on thermalization of the neutrinos in the universe with low reheating temperature, Phys. Rev. D **72**, 043522 (2005).
[107] F. De Bernardis, L. Pagano, and A. Melchiorri, New constraints on the reheating temperature of the universe after WMAP-5, Astropart. Phys. **30**, 192 (2008).
[108] P. F. de Salas, M. Lattanzi, G. Mangano, G. Miele, S. Pastor, and O. Pisanti, Bounds on very low reheating scenarios after Planck, Phys. Rev. D **92**, 123534 (2015).
[109] Planck Collaboration, Planck 2018 results. X. Constraints on inflation, Astrophys. Space Sci. **364**, 69 (2019).
[110] R. Easther, R. Galvez, O. Özsoy, and S. Watson, Supersymmetry, nonthermal dark matter and precision cosmology, Phys. Rev. D **89**, 023522 (2014).
[111] W. H. Kinney and A. Riotto, Theoretical uncertainties in inflationary predictions, J. Cosmol. Astropart. Phys. 03 (2006) 011.
[112] P. Adshead, R. Easther, J. Pritchard, and A. Loeb, Inflation and the scale dependent spectral index: Prospects and strategies, J. Cosmol. Astropart. Phys. 02 (2011) 021.
[113] K. Redmond, A. Trezza, and A. L. Erickcek, Growth of dark matter perturbations during kination, Phys. Rev. D **98**, 063504 (2018).
[114] J. Fan, O. Özsoy, and S. Watson, Nonthermal histories and implications for structure formation, Phys. Rev. D **90**, 043536 (2014).
[115] K. Redmond and A. L. Erickcek, New constraints on dark matter production during kination, Phys. Rev. D **96**, 043511 (2017).
[116] M. Artymowski, M. Lewicki, and J. D. Wells, Gravitational wave and collider implications of electroweak baryogenesis aided by non-standard cosmology, J. High Energy Phys. 03 (2017) 066.
[117] J. Silk, Cosmic black body radiation and galaxy formation, Astrophys. J. **151**, 459 (1968).
[118] M. Breitbach, J. Kopp, E. Madge, T. Opferkuch, and P. Schwaller, Dark, cold, and noisy: Constraining secluded hidden sectors with gravitational waves, J. Cosmol. Astropart. Phys. 07 (2019) 007.
[119] L. Lentati *et al.*, European Pulsar Timing Array limits on an isotropic stochastic gravitational-wave background, Mon. Not. R. Astron. Soc. **453**, 2576 (2015).
[120] NANOGRAV Collaboration, The NANOGrav 11-year data set: Pulsar-timing constraints on the stochastic gravitational-wave background, Astrophys. J. **859**, 47 (2018).
[121] LIGO Scientific and Virgo Collaborations, GW170817: Implications for the Stochastic Gravitational-Wave Background from Compact Binary Coalescences, Phys. Rev. Lett. **120**, 091101 (2018).
[122] LIGO Scientific and Virgo Collaborations, A search for the isotropic stochastic background using data from Advanced LIGO's second observing run, arXiv:1903.02886.
[123] L. A. Boyle and A. Buonanno, Relating gravitational wave constraints from primordial nucleosynthesis, pulsar timing,

laser interferometers, and the CMB: Implications for the early Universe, Phys. Rev. D **78**, 043531 (2008).

[124] A. Stewart and R. Brandenberger, Observational constraints on theories with a blue spectrum of tensor modes, J. Cosmol. Astropart. Phys. 08 (2008) 012.

[125] K. Kohri and T. Terada, Semianalytic calculation of gravitational wave spectrum nonlinearly induced from primordial curvature perturbations, Phys. Rev. D **97**, 123532 (2018).

[126] L. Pagano, L. Salvati, and A. Melchiorri, New constraints on primordial gravitational waves from Planck 2015, Phys. Lett. B **760**, 823 (2016).

[127] P. D. Lasky *et al.*, Gravitational-Wave Cosmology across 29 Decades in Frequency, Phys. Rev. X **6**, 011035 (2016).

[128] LIGO Scientific and Virgo Collaborations, An upper limit on the stochastic gravitational-wave background of cosmological origin, Nature (London) **460**, 990 (2009).

[129] Planck Collaboration, Planck 2018 results. VI. Cosmological parameters, arXiv:1807.06209.

[130] D. Baumann, Inflation, in Physics of the large and the small, TASI 09, *Proceedings of the Theoretical Advanced Study Institute in Elementary Particle Physics, Boulder, Colorado, USA, 2009* (2011), pp. 523–686.